

Moisture sources and dynamics over southeastern Tibetan Plateau reflected in dual water vapor isotopes

Zhongyin Cai^{1*}, Rong Li¹, Cheng Wang¹, Qiukai Mao¹, Lide Tian¹

¹Institute of International Rivers and Eco-security, Yunnan Key Laboratory of International Rivers and Transboundary Eco-security, Ministry of Education Key Laboratory for Ecoscurity of Southwest China, Yunnan University, Kunming, China

*Corresponding author: Zhongyin Cai (czyipil@gmail.com and z.cai@ynu.edu.cn)

Abstract

The southeastern Tibetan Plateau (SETP) has experienced a significant drying trend in recent decades, likely linked to shifts in moisture sources. To investigate the role of ocean surface evaporation, continental air mass intrusion, and rain-vapor interaction, we present a three-year daily time series of near-surface vapor $\delta^{18}\text{O}$ and d -excess from the SETP station. Our analysis reveals that apparent negative correlations between d -excess and relative humidity over the Indian Ocean are primarily driven by similar seasonal patterns, which become insignificant or marginal when examined seasonally. This result underscores the need for caution in interpreting d -excess as a conservative tracer of ocean surface evaporation. Instead, we identify local and upstream specific humidity as the primary determinant of non-monsoon season d -excess variability, influenced by the intrusion of cold and dry air from upper levels. During the summer monsoon season, both d -excess and $\delta^{18}\text{O}$ reflect the effect of raindrop

删除了: change

删除了: Water vapor isotopes are valuable tracers of the atmospheric water cycle, yet their interpretation is hindered by ambiguities in atmospheric controls.

26 evaporation during transport, which decreases $\delta^{18}\text{O}$ but increases d -excess. These findings ~~offer~~ new insights into
27 ~~using~~ water isotopes to track moisture sources and dynamics ~~across~~ SETP, ~~especially~~ under varying seasonal
28 circulation systems. Particularly, the findings for d -excess will contribute to our understanding of different moisture
29 sources and provide a framework for interpreting d -excess in various hydroclimatic applications, including ice core
30 studies.

删除了: provide

删除了: the use of

删除了: over the

删除了: particularly

32 1 Introduction

33 The Tibetan Plateau (TP) and its surrounding regions, known as the Third Pole and the Asian Water Tower, ~~is~~
34 ~~a critical source of freshwater for billions of people~~ (Immerzeel et al., 2020; Yao et al., 2022). ~~Recent climate change~~
35 ~~has induced significant hydrological shifts, marked by drying trends in~~ the southeastern TP (SETP) ~~and~~ wetting in
36 the north (Jiang et al., 2023; Zhang et al., 2023; Yao et al., 2022). Atmospheric water vapor is the primary input to
37 the hydrological system, making it essential to understand its sources and dynamics to diagnose regional water
38 imbalances. Using a Lagrangian vapor tracking method, Zhang et al. (2023) suggested that the drying trend is
39 associated with meteorological droughts propagating from moisture source regions. However, their conclusions and
40 methodology are subjects of ongoing debate (Zhang et al., 2025; Zhao et al., 2025). ~~underscoring the need for~~
41 ~~alternative approaches. As natural tracer of the water cycle, water stable isotopes offer~~ valuable insights into
42 moisture sources and dynamics (Bowen et al., 2019; Galewsky et al., 2016). ~~However, the interpretation of these~~
43 isotopic signals ~~on the TP~~ remains challenging due to complex fractionation processes and shifting circulation
44 systems between summer monsoon and westerlies (Yao et al., 2013; Thompson et al., 2024; Bershaw, 2018; Li et
45 al., 2025).

删除了: plays a crucial role in supplying water to major Asian rivers, including the Mekong, Salween, Ganges, Yarlung Zangbo, among others, sustaining ecosystems and populations across the continent

删除了: In recent decades, the water balance on the TP has undergone significant changes under the backdrop of global warming (Yao et al., 2022). Notably,

删除了: is experiencing a drying trend while

删除了: Water stable isotopes are natural tracers of the water cycle, offering

删除了: These isotopes have been intensively studied on the TP in precipitation, surface water, and ice cores (Yao et al., 2013; Thompson et al., 2024; Bershaw, 2018).

46 Recent studies have confirmed that monsoon convection at upstream along moisture transport pathways, rather

64 than local precipitation amount, controls summer monsoon season precipitation $\delta^{18}\text{O}$ over southern TP (Cai et al.,
65 2017; He et al., 2015). This is related to the “amount effect” (Dansgaard, 1964), where higher precipitation leads to
66 lower $\delta^{18}\text{O}$ values due to continuous rainout associated with stronger convection, following the Rayleigh distillation
67 (Kurita et al., 2015; Ruan et al., 2019; Cai et al., 2025). Additionally, interactions between rain and water vapor play
68 a significant role in depleting the lower tropospheric vapor isotopes (Risi et al., 2008a; Kurita et al., 2011; Cai et al.,
69 2018; Lee and Fung, 2008). While the regional amount effect prevails during the monsoon season, this relationship
70 weakens or reverses in the non-monsoon season when it is dominated by westerlies. This variability suggests
71 additional controls such as moisture source variability, kinetic fractionation, or shifts in atmospheric circulation
72 patterns (Breitenbach et al., 2010; Cai and Tian, 2020; Guo et al., 2024; Yao et al., 2013).

73 Observations of vapor isotopes could help disentangle the different processes involved in the amount effect,
74 particularly through examining the secondary parameter deuterium excess (*d*-excess). The *d*-excess, defined by
75 Dansgaard (1964) as $\delta^2\text{H} - 8\delta^{18}\text{O}$, primarily reflects the effects of kinetic fractionation. During rainout process,
76 equilibrium fractionation is the dominant mechanism, whereas raindrop evaporation is associated with kinetic
77 fractionation. Further, limited precipitation during non-monsoon seasons makes it challenging to study a full
78 seasonal cycle of the atmospheric water cycle, which can be compensated by continuous monitoring of vapor
79 isotopes. While a few stations on the TP have monitored isotopic compositions in the vapor phase (Tian et al., 2020;
80 Dai et al., 2021; Chen et al., 2024; Yu et al., 2016; Yu et al., 2015), there is limited knowledge about vapor *d*-excess.

81 Both theoretical predictions and observations over ocean surfaces indicate that *d*-excess reflects ocean surface
82 evaporation conditions, such as sea surface temperature (SST) and relative humidity normalized to SST (RH_{SST})
83 (Merlivat and Jouzel, 1979; Bonne et al., 2019; Liu et al., 2014; Craig and Gordon, 1965). These relationships are
84 frequently invoked ~~to interpret~~ *d*-excess over the TP (Zhao et al., 2012; Shao et al., 2021; Chen et al., 2024; Liu et
85 al., 2024). For instance, Shao et al. (2021) ~~found~~ significant correlations between an ice core *d*-excess record from

删除了: in interpreting

删除了: showed

88 the central TP and RH_{SS7} over the northern Bay of Bengal (BOB) and Arabian Sea (AS). However, the correlation
 89 coefficient was only -0.44 with a steep slope of $-0.99\% \text{ } ^\circ\text{C}^{-1}$, which differs from the typical range observed in oceanic
 90 regions ($-0.3\% \text{ } ^\circ\text{C}^{-1}$ to $-0.6\% \text{ } ^\circ\text{C}^{-1}$) (Bonne et al., 2019; Liu et al., 2014; Benetti et al., 2014; Uemura et al., 2008).
 91 This discrepancy suggests additional complexities, such as continental recycling and raindrop evaporation.
 92 Furthermore, many studies at other terrestrial sites have also questioned whether d -excess accurately preserves
 93 evaporation conditions from oceanic source regions (Fiorella et al., 2018; Aemisegger et al., 2014; Welp et al., 2012;
 94 Wei and Lee, 2019; Samuels - Crow et al., 2014).

95 In addition, ice core d -excess values at high altitudes are generally higher than those observed in precipitation
 96 at lower altitudes on the TP (Shao et al., 2021; Tian et al., 2001; Zhao et al., 2012; Joswiak et al., 2013; Zhao et al.,
 97 2017; Thompson et al., 2000). High vapor d -excess values at high elevations have been observed elsewhere, such
 98 as on the Andes (Samuels - Crow et al., 2014). Such elevated d -excess values have been attributed to the mixing
 99 with subsiding air (Samuels - Crow et al., 2014; Sodemann et al., 2017). However, this mechanism remains
 100 unconfirmed on the TP.

101 Mountain valleys in the SETP have been considered as significant pathways for transporting water vapor into
 102 the TP (Araguás-Araguás et al., 1998; Tian et al., 2007; Yao et al., 2013). To investigate these processes, we initiated
 103 a water vapor sampling campaign at the South-East Tibetan Plateau Station for integrated observation and research
 104 of alpine environment (SETP station) in June 2015. The primary objectives were to explore moisture sources and
 105 dynamics and their influence on vapor isotope compositions across different seasons. To achieve these goals, we
 106 analyzed the relationships between vapor isotopes and oceanic evaporation conditions, continental air mass
 107 intrusions, as well as rain-vapor interactions during different seasons. Finally, we discuss how our findings
 108 contribute to the interpretation of ice core records.

删除了: . This contrasts with

删除了: where the slope typically ranges from

删除了:

删除了: (Bonne et al., 2019; Liu et al., 2014; Benetti et al., 2014; Uemura et al., 2008),

删除了: suggesting

删除了: over terrestrial areas

删除了: Moreover

删除了: suggested that d -excess at terrestrial sites is not a conservative tracer of

删除了: evaporation conditions from oceanic source regions

删除了: (Webster and Heymsfield, 2003)

删除了: The reason for this discrepancy remains unclear, highlighting the need for further research to understand the mechanism driving these differences.

删除了: are

删除了: We aim to study

删除了: the

删除了: explored

删除了: the implications of our findings for interpreting

129 **2 Data and methods**

130 **2.1 Atmospheric water vapor sampling**

131 Vapor samples were collected at the SETP station (29°46'N, 94°44'E, 3326 m above sea level, and Fig. S1)
132 using a cryogenic trapping method. The sampling system includes an air pump, a linked-ball-shaped glass cold trap,
133 and an electric-powered system that creates and maintains a cold environment filled by 95% ethanol as cold as
134 below -80 °C. Ambient air was pumped from an inlet positioned about 8 m above ground level through a Teflon
135 tube to a glass trap maintained at an operational temperature of -70 °C. The airflow rate was set to ~5 L/min,
136 allowing the collection of 10-20 ml of water samples during each sampling session. Sampling durations were
137 adjusted seasonally: 24 hours in summer and extended to 48 hours in winter when necessary to ensure adequate
138 sample volume. Samples were collected at 20:00 Beijing Standard Time (12:00 UTC). The efficiency of the trapping
139 method was verified by connecting an additional cold trap to the system, which showed no visible condensation in
140 the additional cold trap (Yu et al., 2015). Further validation was achieved through comparisons with direct
141 measurements using a Picarro L2130-i Cavity Ring Down Spectroscopy (CRDS) at Lhasa, southern TP, confirming
142 the reliability of this method for atmospheric water vapor sampling (Tian et al., 2020).

143 The sampling campaign ran from 25 June 2015 to 14 June 2018, yielding a total of 742 samples. These samples
144 were stored frozen until analysis. ~~Those collected before 28 June 2016 were measured at the Key Laboratory of~~
145 Tibetan Plateau Earth System, Environment and Resources, Institute of Tibetan Plateau Research, Chinese Academy
146 of Sciences by a Picarro L2130-i analyzer. Samples collected after 28 June 2016 were measured at the Institute of
147 International River and Eco-security, Yunnan University by a Picarro L2140-i analyzer. The isotopic values were
148 calibrated using three standard waters, with detailed calibration procedures described by Liu et al. (2024). The
149 measurements are expressed relative to Vienna Standard Mean Ocean Water 2 (VSMOW2), with precisions of 0.1‰
150 for $\delta^{18}\text{O}$, 0.4‰ for $\delta^2\text{H}$, and 1.2‰ for d -excess.

删除了: Samples

152 2.2 Meteorological data

153 Daily local meteorological data prior to 2018, including precipitation amount, air temperature, air pressure,
154 and relative humidity at the SETP station, were obtained from the National Tibetan Plateau/Third Pole Environment
155 Data Center (Luo, 2018). Specific humidity (q) at the SETP station was calculated using air temperature, air pressure,
156 and relative humidity data following established equations outlined in (Huang, 2018). ▽

157 We further obtained meteorological variables such as 2-meter air temperature, 2-meter dew point temperature,
158 SST, and others at $0.25^\circ \times 0.25^\circ$ and hourly resolution from the European Centre for Medium-Range Weather
159 Forecasts fifth generation reanalysis (ERA5) (Hersbach et al., 2019). RH_{SST} is estimated using ERA5 data: $RH_{SST} =$
160 e_{air}/e_{sat} , where e_{air} is vapor pressure of air and e_{sat} is saturation vapor pressure with respect to SST.
161 Additionally, precipitation data at $0.1^\circ \times 0.1^\circ$ and half-hourly resolution were obtained from the Integrated Multi-
162 satellitE Retrievals for GPM (V07) dataset (Huffman et al., 2023). Moreover, we used ERA5 data and
163 meteorological data at $1^\circ \times 1^\circ$ and 3-hourly resolution from the Global Data Assimilation System (GDAS) to ▽
164 calculate backward trajectories (see Section 2.4 for details).

165 Statistical analyses primarily involved linear correlations and regressions, with the coefficient of determination
166 (R^2) used to quantify the variance explained by each variable. In addition, we also used composite analysis to reveal
167 relationships between variables. For example, to identify general patterns in backward trajectories associated with
168 d -excess exceeding 30‰, all the days with such high d -excess were compiled into a collection. A composite map of
169 trajectories from this collection was then constructed to reveal typical pathways under these conditions.

170 2.3 Theoretical framework for the understanding of isotope compositions and humidity

171 Besides complex atmospheric circulation models, the evolution of vapor isotope compositions during different
172 moistening and dehydration processes can be predicted through a compilation of atmospheric processes such as
173 condensation, mixing, and raindrop evaporation (Noone, 2012; Worden et al., 2007; Galewsky et al., 2016). These

删除了: Consistent with Yao et al. (2013), we defined June-September (JIAS) as the summer monsoon season. In contrast, November-April (Nov-Apr) was designated as the non-monsoon season, with May and October considered transition periods between the two seasons.

删除了: were used

180 process shape distinct pathways of isotopic evolution in relation to atmospheric humidity.

181 The Rayleigh distillation model describes the progressive condensation of water vapor (Dansgaard, 1964). The
182 isotope composition of remaining vapor, denoted as δ , can be expressed as $\delta = (1 + \delta_0)(q/q_0)^{\alpha-1} - 1$, where q
183 is the specific humidity, and α is the fractionation factor. A subscript of 0 refers to the initial condition of the air
184 mass. Raindrop evaporation introduces further complexity. As raindrops form at higher altitudes where vapor is
185 depleted in heavy isotopes, their partial evaporation affects the surrounding vapor, leading to isotope values lower
186 than those predicted by Rayleigh models (Risi et al., 2008a; Worden et al., 2007). This effect gives rise to “super-
187 Rayleigh” trajectories, characterized by an inflated effective fractionation factor (α_e), defined as $\alpha_e = (1 + \phi)\alpha$,
188 where ϕ quantifies deviations from equilibrium. Notably, Worden et al. (2007) and Noone (2012) have given
189 different equations for such deviations, and this study aligns with the formulations by Noone (2012).

190 Air mass mixing also influences humidity and isotopic compositions. When a dry air mass mixes with a moist
191 one, the specific humidity of the mixed air can be described as $q = f_{dry}q_{dry} + f_{moist}q_{moist}$, where f represents
192 the fraction of each air mass, with $f_{dry} + f_{moist} = 1$. Isotopic compositions are similarly derived by solving mass
193 balance equations for the light and heavy isotopes, resulting in a hyperbolic relationship between δ and q . In other
194 words, $\delta \times q$ and q should have a linear relationship in the mixing process (Fiorella et al., 2018). The intercept
195 of the regression between δ and $1/q$ or the slope between $\delta \times q$ and q provides an estimate of the moist end
196 member’s isotope composition (Keeling, 1958).

197 Assuming a surface temperature of 25 °C and relative humidity of 85%, we utilize the evaporation model by
198 Craig and Gordon (1965) to determine the isotopic composition of ocean evaporation. This results in $\delta^{18}\text{O} = -11.5\text{‰}$,
199 $\delta^2\text{H} = -81.4\text{‰}$, and $d\text{-excess} = 10.6\text{‰}$. These values serve as the wet end member for modeling moistening process
200 through mixing with ocean evaporation. For the dry end member, we consider a dehydrated air mass from the
201 Rayleigh curve at $q = 0.5 \text{ g/kg}$, $\delta^{18}\text{O} = -60.3\text{‰}$, and $\delta^2\text{H} = -418.0\text{‰}$ (Fig. S2). The dehydration process via

删除了: through mass balance principles

condensation is initiated at a relative humidity of 80% on the mixing line. Similarly, “super-Rayleigh” distillation involving partial rain evaporation also begins from this starting point. We explore two “super-Rayleigh” scenarios: Rain_evap_A assumes 2% rain evaporation, while Rain_evap_B assumes 5%, based on equations from Noone (2012). Additionally, we consider the influence of evapotranspiration over south Asia and the TP on atmospheric humidity and vapor isotope compositions over SETP. Quantifying isotopic compositions of land surface evapotranspiration is challenging. Given precipitation $\delta^{18}\text{O}$ over south Asia generally ranges from -1.0‰ to -5.0‰ (Bowen and Wilkinson, 2002; Terzer-Wassmuth et al., 2021) and transpiration constitutes two-thirds or more of evapotranspiration (Cao et al., 2022; Han et al., 2022; Good et al., 2015), we assume a $\delta^{18}\text{O}$ value of -5.0‰ as an upper bound for land surface evapotranspiration. Similarly, we assume a d -excess of 15.0‰ for this wet end member.

2.4 Backward trajectory and moisture source diagnostic

To investigate air mass transport and diagnose moisture sources and pathways toward SETP, we calculated backward trajectories using the Hybrid Single-Particle Lagrangian Integrated Trajectory model (HYSPLIT) (Stein et al., 2015). Trajectory calculations were driven by nested ERA5 (within the domain of 0-50°N and 40-120°E) and GDAS (globally but when outside of the ERA5 domain) data, to achieve higher resolution in the major potential source regions. In addition, the vertical motion was also driven by the model vertical velocity. Air parcels were released from 5 locations: the study site and points displaced 0.2° in each cardinal direction. These releases occurred at 7 different vertical levels: 10, 50, 100, 200, 300, 400, and 500 m above ground level. For each day during the sampling campaign, trajectories were initiated every 3 hours to calculate 10-day backward trajectories, resulting in 280 trajectories per day. Geographical and meteorological variables, including location, pressure, temperature, specific humidity, rainfall amount, boundary layer height, and terrain height along the trajectories, were stored at hourly intervals.

To quantify moisture contributions along trajectories to SETP’s humidity, we applied the Lagrangian moisture

删除了: meteorological data from the

删除了: .

227 source diagnostic method developed by Sodemann et al. (2008). This method uses mass balance principles along
228 trajectories, interpreting increases in specific humidity (forward in time) as moisture uptake and decreases as
229 moisture loss due to precipitation. It also accounts for the reduced contribution of earlier moisture uptake due to
230 precipitation en route. We previously adapted this method to identify moisture sources for precipitation in sub-
231 regions of South Asia and East Asia (Cai et al., 2018; Cai and Tian, 2020).

232 In this framework, the moisture source can be attributed into four categories: contributions within an extended
233 boundary layer over 1) land and 2) ocean, 3) contributions from above the extended boundary layer, and 4)
234 remaining unattributed sources. Following Sodemann et al. (2008), the extended boundary layer was parameterized
235 as 1.5 times the boundary layer height. The diagnostic results indicated that approximately 7.0% of the moisture
236 arriving at SETP remained unattributed, confirming that 10-day trajectories are sufficient to diagnose most moisture
237 sources. Overall, the fractions of within-boundary-layer contributions are 60.2% over land and 5.0% over ocean,
238 with an additional 27.8% originating from above the extended boundary layer. Additionally, this study emphasizes
239 the contribution of air parcels themselves to SETP's humidity. This variable captures the history of the moisture and
240 indicates how much moisture within each air parcel finally reaches SETP.

241 The moisture contribution of an air parcel to SETP's humidity is a measure of the importance of upstream air.
242 We calculated weighted-mean values for key variables by using the moisture contribution of the air parcel along
243 trajectories as the weight. We also applied K-means clustering to group trajectories, helping to identify major
244 transport pathways. When calculating the mean trajectory for each cluster and meteorological variables along each
245 mean trajectory, the moisture contribution of the air parcel is also considered as the weight to calculate weighted-
246 means.

删除了: 5

删除了: Unlike previous applications focused on identifying evaporative moisture sources from the Earth's surface

删除了: This variable is readily available from the diagnostic method, where changes in air parcel contributions within the boundary layer between time steps represent moisture uptake from the surface.

254 **3 Results**

255 **3.1 General characteristics of vapor $\delta^{18}\text{O}$, d -excess, and local meteorological variables**

256 Consistent with Yao et al. (2013), we defined June-September (JJAS) as the summer monsoon season. In
257 contrast, November-April (Nov-Apr) was designated as the non-monsoon season, with May and October considered
258 transition periods between the two seasons. In general, $\delta^{18}\text{O}$ values are at lower levels during the summer monsoon
259 season and higher levels during the non-monsoon season (Fig. 1a). Mean $\delta^{18}\text{O}$ values are -18.4‰ for the non-
260 monsoon season, -23.3‰ for the summer monsoon season, -16.9‰ for May, and -22.8‰ for October. $\delta^{18}\text{O}$ shows
261 a dramatic decrease at the onset of the summer monsoon. Conversely, from the end of the summer monsoon season
262 to spring and early summer, $\delta^{18}\text{O}$ shows a gradual increase trend. Although the amount effect significantly influences
263 this region, the seasonal variation of $\delta^{18}\text{O}$ does not strictly align with local precipitation patterns. For instance, while
264 local precipitation ceases clearly after the summer monsoon (Fig. 1e), $\delta^{18}\text{O}$ remains at relatively low levels. This
265 behavior is consistent with precipitation $\delta^{18}\text{O}$ in SETP, northeast India, and Bangladesh (Yao et al., 2013; Cai and
266 Tian, 2020; Yang et al., 2017).

267 Although d -excess values are also lower during the summer monsoon season and higher during non-monsoon
268 periods, the timing of seasonal transitions differs from that of $\delta^{18}\text{O}$ (Fig. 1b). Mean d -excess values are 18.3‰ for
269 the non-monsoon season, 11.9‰ for the summer monsoon season, 13.7‰ for May, and 14.9‰ for October. The
270 highest d -excess values generally occur during winter months when air temperature and relative humidity (RH) are
271 at their lowest levels (Fig. 1c and 1d). Furthermore, d -excess starts to decrease in spring, earlier than the sharp drop
272 in $\delta^{18}\text{O}$ at the onset of the summer monsoon.

删除了: In contrast to $\delta^{18}\text{O}$, d -excess displays different seasonal dynamics.

删除了: The

删除了: However, the timing of seasonal transitions in d -excess differs from that of $\delta^{18}\text{O}$.

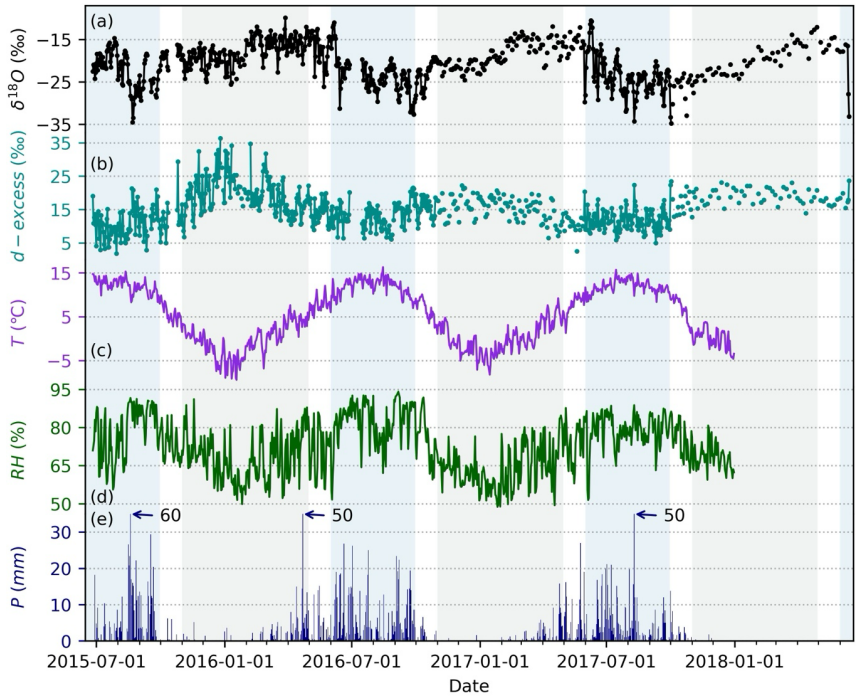
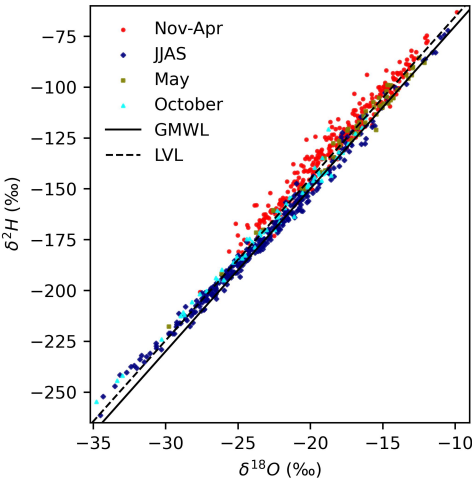


Figure 1. Time series of observed vapor $\delta^{18}\text{O}$, d -excess, and daily local meteorological variables from 2015-2018: (a) $\delta^{18}\text{O}$, (b) d -excess, (c) air temperature, (d) relative humidity (RH), and (e) precipitation amount. Light blue shading highlights the summer monsoon season, while light steel blue shading indicates the non-monsoon season.

The linear relationship between paired $\delta^{18}\text{O}$ and $\delta^2\text{H}$ values, along with their position relative to the global meteoric water line (GMWL, $\delta^2\text{H} = 8\delta^{18}\text{O} + 10$) (Craig, 1961), provides additional insights into isotopic fractionation processes (Putman et al., 2019). The local vapor line (LVL), estimated from all $\delta^2\text{H}$ and $\delta^{18}\text{O}$ data points, is $\delta^2\text{H} = 7.96\delta^{18}\text{O} + 14.04$ ($R^2 = 0.98$). This LVL plots above but approximately parallel with the GMWL. This relatively higher intercept of LVL reflects the continental location of the site and additional kinetic fractionation after ocean evaporation. The $\delta^2\text{H}$ - $\delta^{18}\text{O}$ relationship also varied seasonally. During the non-monsoon season, the LVL

删除了: highlights

290 is $\delta^2\text{H} = 7.58\delta^{18}\text{O} + 10.61$ ($R^2 = 0.96$), while during the summer monsoon season, it shifts to $\delta^2\text{H} = 7.53\delta^{18}\text{O} + 0.91$
291 ($R^2 = 0.99$). Non-monsoon data primarily plot above both the GMWL and the overall LVL. Conversely, most
292 monsoon season isotope data fall below the overall LVL, though the lowest δ -value points during this period are
293 positioned above the overall LVL, suggesting additional kinetic fractionation such as rain evaporation (He et al.,
294 2024). Vapor isotopes for May resemble those of the non-monsoon season but align more closely with both the
295 GMWL and LVL, whereas data for October exhibit behaviors similar to the monsoon season observations.



296
297 **Figure 2. Relationship between vapor $\delta^2\text{H}$ and $\delta^{18}\text{O}$. The data is presented for different seasons: non-**
298 **monsoon (Nov-Apr) as red dots, summer monsoon (JJAS) as navy diamonds, May as olive squares, and**
299 **October cyan triangles. The solid line indicates the global meteoric water line (GMWL). The dashed line**
300 **indicates the local vapor line (LVL) estimated from all $\delta^2\text{H}$ and $\delta^{18}\text{O}$ data points.**

301 The relationships between $\delta^{18}\text{O}$ and specific humidity (q) further indicate distinct seasonal patterns in moisture
302 dynamics (Fig. 3a). Due to unavailability of local meteorological data for 2018, our analyses focused on data
303 collected before this year. During the non-monsoon season, particularly in winter months, most data points are
304 positioned above the Rayleigh distillation line but below a mixing line that represents an upper bound of

删除了: triangles

删除了: .

307 hypothetical evapotranspiration over South Asia. This suggests a mix between a dry end member and a moist end
308 member. In contrast, during the summer monsoon season, data predominately fall below the Rayleigh line,
309 influenced by “super-Rayleigh” processes linked to rain evaporation.

310 Further insights come from examining $\delta \times q$ versus q relationships, which highlight seasonal contrasts in
311 moisture source signatures (Fig. S3). For the non-monsoon season, a simple estimation through the linear regression
312 between $\delta \times q$ and q suggests a moist end member with an $\delta^{18}\text{O}$ of $-13.9\text{‰} \pm 0.6\text{‰}$. The amount weighted annual
313 mean precipitation $\delta^{18}\text{O}$ at our site was about -14.5‰ (Yao et al., 2013). However, during the monsoon season, the
314 overall estimation of $\delta^{18}\text{O}$ for the moist end member through the linear regression between $\delta \times q$ and q is
315 significantly lower at $-30.9\text{‰} \pm 1.8\text{‰}$, pointing to an additional moisture source from rain evaporation that is more
316 depleted in heavy isotopes. These results align with the distribution of $\delta^{18}\text{O}$ - q data below the Rayleigh line during
317 the summer monsoon season (Fig. 3a), underscoring the influence of different moisture sources and processes across
318 seasons.

319 The relationships between d -excess and q also reflect seasonal contrasts in moisture dynamics (Fig. 3b). During
320 non-monsoon season months, a negative correlation is observed where lower q corresponds to higher d -excess
321 values (Figs. 1 and 3b). This relationship is particularly pronounced under dry and cold conditions. In contrast,
322 during the summer monsoon season, no clear relationship between d -excess and q is apparent, with d -excess
323 showing considerable variability of approximately 20‰ at any given q . These findings suggest that d -excess is less
324 predictable using q compared to $\delta^{18}\text{O}$, except under low humidity levels.

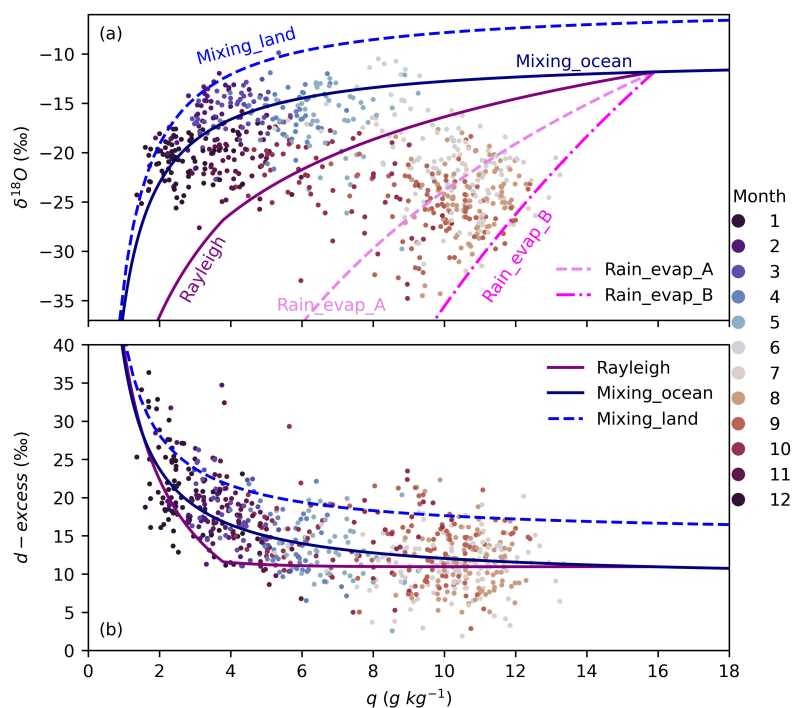


Figure 3. Relationships between vapor isotopes ($\delta^{18}\text{O}$ and d -excess) and specific humidity (q) from 2015-2017. (a) scatter plot of $\delta^{18}\text{O}$ against q . (b) scatter plot of d -excess against q . Each data point is color-coded by month. Reference lines correspond to those in Fig. S2; their interpretations are detailed in Fig. S2 and Section 2.3. Note that only data before 2018 are shown (see text for details).

删除了: is

3.2 Seasonal variability in moisture sources and transport pathways

To understand the drivers behind the seasonal variations in moisture dynamics, we analyzed the moisture sources and transport pathways during different seasons (Fig. 4). Our focus was on the contribution of moisture from historical air masses (last 10 days) to humidity at SETP.

During the non-monsoon season (Fig. 4a), moisture is mainly transported via two pathways: one originating from the west of SETP, carried by the westerlies (clusters Nov-Apr2 and Nov-Apr3), and another from the south,

337 such as the BOB (cluster Nov-Apr1). Quantitatively, the contribution is 84.8% from the southern pathway and 15.2%
338 from the western branches combined. Interestingly, when considering only trajectories without accounting for
339 moisture contributions, all three clusters appear to originate from the west or southwest of SETP (Fig. S4). This
340 discrepancy highlights the importance of distinguishing between pure air mass transport and actual moisture sources
341 when interpreting trajectory data.

342 In contrast, during the summer monsoon season (Fig. 4b), moisture transport is predominantly from the south
343 of SETP, driven by the summer monsoon. The pathways observed in May (Fig. 4c) represent a transition from the
344 non-monsoon season (Fig. 4a) toward the dominant southerly transport seen during the summer monsoon (Fig. 4b).
345 In comparison, the moisture sources and transport pathways exhibit a slight eastward shift during October compared
346 with those during the summer monsoon season (Figs. 4d and S4d).

347 Another notable aspect of the moisture source distributions is the dominant contribution from proximal
348 terrestrial regions, particularly those to the south of SETP (Fig. 4). For example, the 1% contour representing
349 moisture contributions from air parcels over each 1°×1° grid box does not or barely extend into oceanic regions
350 during any of the four seasons. This indicates that surface evaporation from oceanic regions such as the BOB and
351 AS contributes minimally. Quantitatively, the within-boundary-layer contributions from oceanic regions are
352 determined to be 2.5%, 9.1%, 4.6%, and 2.0% for non-monsoon, summer monsoon, May, and October, respectively.
353 Most of the moisture originating over these oceanic regions is lost through precipitation before reaching SETP, and
354 what remains is replenished by evapotranspiration during transport over land. This finding raises an important
355 question: do the vapor isotopes measured at SETP still reflect the meteorological conditions at their oceanic sources?

删除了: s

删除了: from these pathways are comparable, with 52.4%

删除了: 47.7

删除了: share similarities with those of the non-monsoon season, but with notable differences. Specifically, the second pathway during May (cluster May2) shifts southward toward the AS compared to its counterpart during the non-monsoon (cluster Nov-Apr2)...

删除了: Similarly, while October's air mass transport direction mirrors that of the non-monsoon, the moisture sources and pathways show greater alignment with those of the summer monsoon season, albeit with

删除了: Instead, m

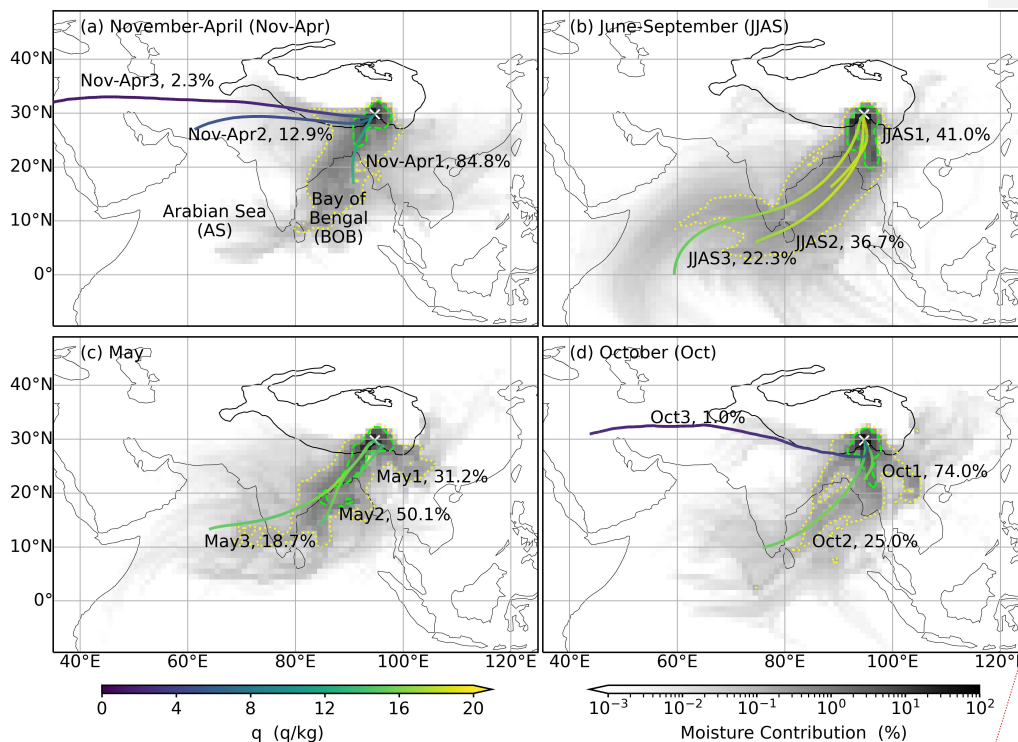
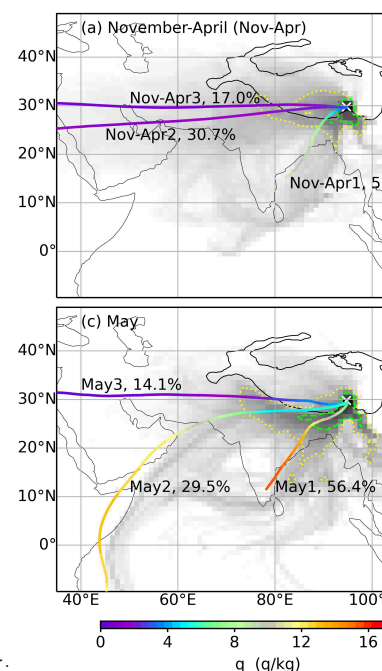


Figure 4. Moisture sources and transport pathways during different seasons from 2015-2017. (a) spatial distribution of relative contributions of moisture from all air parcels over each $1^{\circ} \times 1^{\circ}$ box (shading) to humidity at the SETP station, along with specific humidity (q) along mean trajectories (weighted by moisture contributions) for the non-monsoon season of November-April (Nov-Apr). (b-d) are the same as (a), but for the monsoon season of June-September (JJAS, b), May (c), and October (d), respectively. The dotted yellow and dashed green contours indicate the moisture contribution at 0.1% and 1%, respectively. The yellow crosses indicate the location of the SETP station. The black solid lines denote the Tibetan Plateau with altitude contour at 3000 m.



删除了:

删除了: respectively

3.3 Role of ocean surface evaporation conditions at seasonal and intraseasonal time scales

Relationships between d -excess and ocean surface evaporation conditions, such as RH_{SST} and SST, were examined using data from 2015-2017 (Fig. 5a and Fig. S5a). Results indeed show negative correlations between d -excess and RH_{SST} over northern Indian Ocean, particularly in the northern parts of AS and BOB (Fig. 5a). Specifically, the regression slopes for this relationship across the northern Indian Ocean vary from higher than $-0.1\% \text{ } ^\circ\text{C}^{-1}$ to values below $-0.6\% \text{ } ^\circ\text{C}^{-1}$.

Focusing on specific regions, the northern BOB (10-22°N and 80-99°E) and the eastern AS (7-20°N and 65-78°E; Fig. 5a) exhibited regression slopes within the range (from $-0.3\% \text{ } ^\circ\text{C}^{-1}$ to $-0.6\% \text{ } ^\circ\text{C}^{-1}$) previously reported (Uemura et al., 2008; Benetti et al., 2014; Liu et al., 2014; Bonne et al., 2019). For instance, the regional average RH_{SST} in the eastern AS shows an overall regression slope of $-0.49\% \text{ } ^\circ\text{C}^{-1}$ ($r = -0.52$ and $p < 0.01$) (Fig. 6a), while the northern BOB has a slope of $-0.52\% \text{ } ^\circ\text{C}^{-1}$ ($r = -0.55$ and $p < 0.01$) (Fig. 6b). However, the clustering of data points by season (Fig. 6) suggests that the apparent negative correlations might primarily stem from opposing seasonal trends. Similarly, apparent negative correlations between d -excess and SST also emerge over the northern Indian Ocean (Fig. S5a). Yet, both theoretical prediction (Merlivat and Jouzel, 1979) and in-situ observations above the ocean surface (Bonne et al., 2019; Liu et al., 2014) reveal a positive correlation between d -excess and SST. These discrepancies lead us to speculate that the overall correlations between SETP vapor d -excess and surface evaporation conditions over the northern Indian Ocean are likely driven by seasonal variability.

The relationship between d -excess and RH_{SST} was further analyzed by distinguishing between the summer monsoon and non-monsoon seasons. During the summer monsoon season, the negative correlation diminishes significantly, with correlation coefficients dropping below 0.3 (Fig. 5b). In contrast, significant correlations present during the non-monsoon season (Fig. 5c), potentially due to intraseasonal variations where d -excess peaks in winter and decreases at the beginning and ending of the non-monsoon season (Fig. 1b), possibly accompanied by opposing

删除了: upon closer inspection of the d -excess- RH_{SST} plots (Fig. 6), it becomes evident that data points clustered according to different seasons, implying

删除了: suggest

405 RH_{SST} trends. ~~Although the correlation is significant~~ during the non-monsoon season, the explained variance in *d*-
406 excess remains low, at a maximum of 10%-16% over the northern BOB. Similarly, correlations with SST over the
407 northern Indian Ocean also become negligible when seasons are considered separately (Fig. S5). ~~To account for~~
408 ~~transport time, we examined correlations between *d*-excess and RH_{SST} from 1 to 11 days prior to the *d*-excess~~
409 ~~observation dates during the summer monsoon (Fig. S6) and non-monsoon seasons (Fig. S7), respectively. The~~
410 ~~results are consistent with those shown in Fig. 5, indicating that considering these lagged timeframes does not~~
411 ~~enhance the correlation between *d*-excess and RH_{SST}.~~ In summary, vapor *d*-excess at SETP is less likely a
412 conservative tracer of surface evaporation conditions (neither RH_{SST} nor SST) over the northern Indian Ocean.
413 Therefore, interpreting *d*-excess in meteoric water or paleo archives from the TP as a proxy for Indian Ocean
414 evaporation conditions should be approached with caution.

删除了: However, even

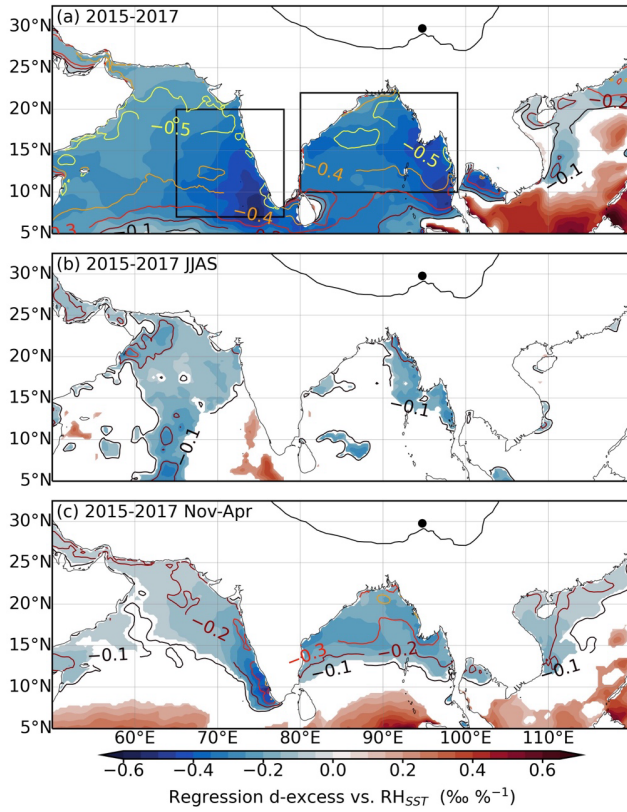


Figure 5. Relationships between vapor d -excess and relative humidity scaled to sea surface temperature (RH_{SST}). (a) regression of d -excess against RH_{SST} (shading and only values significant at the 95% significance level are shown) and correlation coefficients between them (contours at an interval of 0.1 and only negative correlations are shown) for all the data from 2015-2017. (b) and (c) are the same as (a) but only for the data within the summer monsoon season (JJAS) or the non-monsoon season (Nov-Apr), respectively. The black dots indicate the location of the SETP station. The black solid lines denote the Tibetan Plateau with altitude contour at 3000 m.

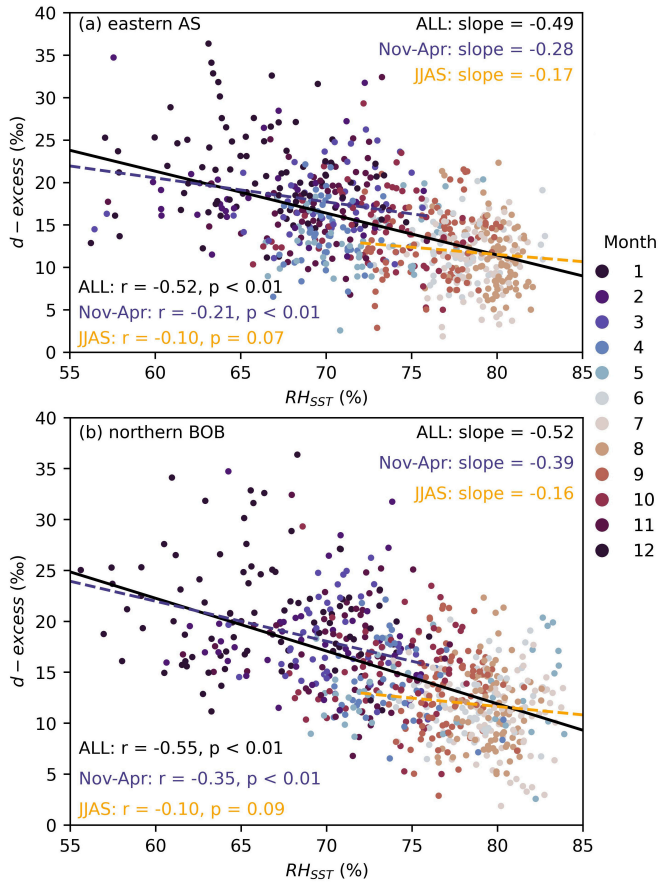


Figure 6. Relationships between SETP vapor d -excess and relative humidity normalized to sea surface temperature (RH_{SST}) averaged over (a) eastern Arabian Sea (7-20°N and 65-78°E) and (b) Bay of Bengal (10-22°N and 80-99°E) from 2015-2017. Each data point is color-coded by month. Solid black lines indicate the linear regression between all data points. Dashed orange lines indicate linear regression for data during the non-monsoon season (Nov-Apr) and dashed dark blue lines for data during the summer monsoon (JJAS). The slope (‰ %⁻¹), r , and p values for the three data groups are also shown.

431 **3.4 Role of dry and cold air intrusion during the non-monsoon season**

432 Both theoretical predictions from the Rayleigh model and observations during the non-monsoon season suggest
433 that d -excess increases as q decreases when q reaches extremely low values (Fig. 2). In addition, results for both air
434 mass transport and moisture transport show the significant role of the westerlies (Figs. S4a and 4a). Based on these
435 evidences, we propose that during the non-monsoon season, vapor isotopes are influenced by the mixing of cold
436 and dry air transported by westerlies from higher altitudes with surface vapor. Furthermore, surface vapor influenced
437 by recycled moisture from terrestrial evapotranspiration would further elevate d -excess at a given q (Fig. 3b).

438 We performed a composite analysis on moisture sources and transport pathways for the highest (higher than
439 30%, and $n = 10$) and lowest (lower than 10%, and $n = 8$) d -excess observations during the non-monsoon season
440 (Fig. 7). High d -excess values are primarily associated with moisture transported by westerlies from regions west
441 or southwest of SETP, such as over the TP and northem India. In addition, backward trajectories for these cases
442 show air masses characterized by extremely low q , reaching below 2 g kg^{-1} along the mean trajectories (weighted
443 by moisture contribution) over the TP (Fig. 7a). Conversely, for low d -excess cases, the moisture transport pathways
444 shift toward more humid regions south of SETP, including northeast India, Bangladesh, and the BOB (Fig. 7b). This
445 contrasting moisture transport pattern between high and low d -excess cases aligns with our hypothesis that high d -
446 excess is associated with dry and cold air transported by westerlies.

删除了: dominant

删除了: western

删除了: a significant portion of

删除了: s

删除了: , with the L1 cluster accounting for 39.2%

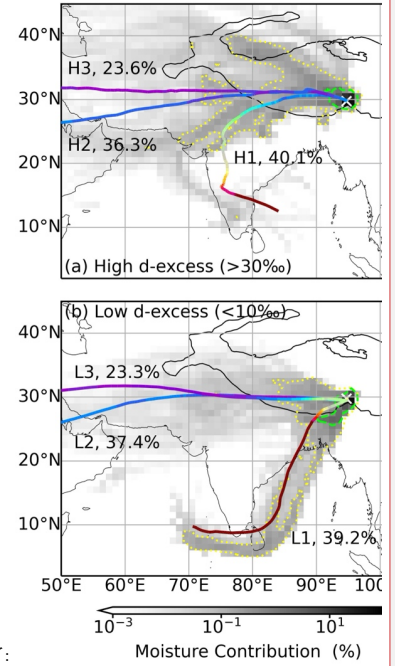
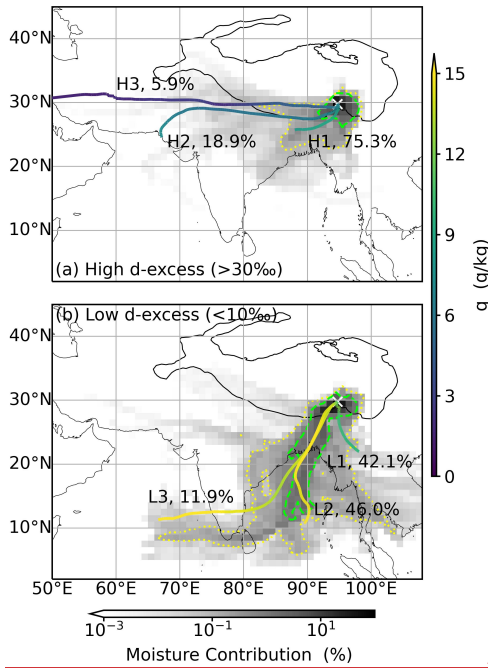


Figure 7. Composite of moisture sources and transport pathways for high and low d -excess days during the non-monsoon season of November–April. (a) spatial distribution of relative contribution of moisture from all air parcels over each $1^\circ \times 1^\circ$ box (shading) to humidity at the SETP station, along with specific humidity (q) along mean trajectories (weighted by moisture contributions) for d -excess values higher than 30‰ during the non-monsoon season ($n = 10$). (b) is the same as (a) but for d -excess lower than 10‰ ($n = 8$). The yellow crosses indicate the location of the SETP station. The black solid lines denote the Tibetan Plateau with altitude contour at 3000 m.

The influence of cold and dry air intrusions was further investigated through an analysis of relationships involving d -excess, local q , weighted-mean upstream q , weighted-mean upstream air temperature, and weighted-mean upstream air altitude (Fig. 8). Upstream variables represent weighted averages along the 10-day backward trajectory, where weights correspond to the moisture contribution at each time step (Section 2.4). The non-monsoon

465 season d -excess shows robust negative correlations with both local q ($r = -0.65$, $p < 0.01$; Fig. 8a) and upstream q
 466 ($r = -0.48$, $p < 0.01$). Furthermore, local q is strongly linked with upstream q ($r = 0.83$, $p < 0.01$; Fig. 8b), which is
 467 associated with air masses characterized by low temperatures and high altitudes (Figs. 8c and 8d). Additionally, the
 468 properties of the upstream air, could also impact $\delta^{18}\text{O}$. Indeed, $\delta^{18}\text{O}$ during high d -excess cases is lower than during
 469 low d -excess cases (at a significance level of 95.3%). The overall correlation coefficient between $\delta^{18}\text{O}$ and d -excess
 470 during the non-monsoon season is -0.29 ($p < 0.01$). Notably, correlations between $\delta^{18}\text{O}$ and q are weaker compared
 471 to those observed for d -excess, with local q showing $r = 0.42$ ($p < 0.01$) and upstream q showing $r = 0.41$ ($p < 0.01$).
 472 The relationship between non-monsoon season $\delta^{18}\text{O}$ and humidity is mainly expressed as the relationship between
 473 $\delta \times q$ and q ($r = 0.82$ for local q and $r = 0.80$ for upstream q). Spatial correlations between vapor isotopes ($\delta^{18}\text{O}$
 474 and d -excess) and 2-meter air temperature as well as humidity measured by 2-meter dew point temperature also
 475 support these findings (Fig. S8). Significant negative correlations between d -excess and dew point temperature exist
 476 over southeastern TP, northeast India, and northern Bangladesh. In contrast, $\delta^{18}\text{O}$ shows significant positive
 477 correlations with air temperature over the India subcontinent and northwestern Southeast Asia.
 478 As shown in Fig. 3b, extremely high d -excess values are predicted at very low q levels. Previous studies have
 479 shown that as q approaches zero, vapor d -excess can approach 7000‰ following the Rayleigh distillation trajectory
 480 (Bony et al., 2008), a behavior inherent to the definition of d -excess (Dütsch et al., 2017). High d -excess values
 481 have also been observed in low humidity environments, like polar regions (Bonne et al., 2014; Steen-Larsen et al.,
 482 2017) and high altitudes (Samuels - Crow et al., 2014; Sodemann et al., 2017; Webster and Heymsfield, 2003).
 483 Therefore, we infer that the increasing trend of d -excess with decreasing local q , upstream q , and regional dew point
 484 temperature is due to enhanced mixing with dry and cold subsiding air transported by westerlies from high altitudes.
 485 Relationships between upstream q and upstream air temperature as well as altitude further support this inference,
 486 indicating that low humidity conditions are associated with the presence of subsiding dry and cold air from high

删除了: 67

删除了: low

删除了: , which

删除了: 38

删除了: 90

删除了: S6

删除了: such as

altitudes (Figs. 8c and 8d). Therefore, vapor d -excess during the non-monsoon not only provides insights into specific humidity levels but also indicates the source of humidity.

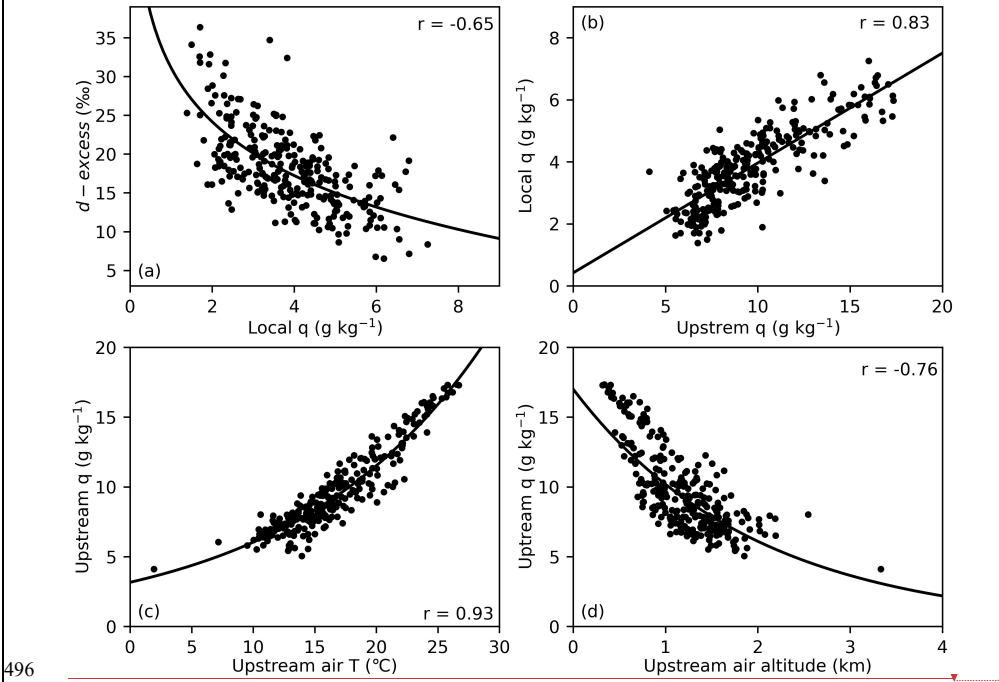
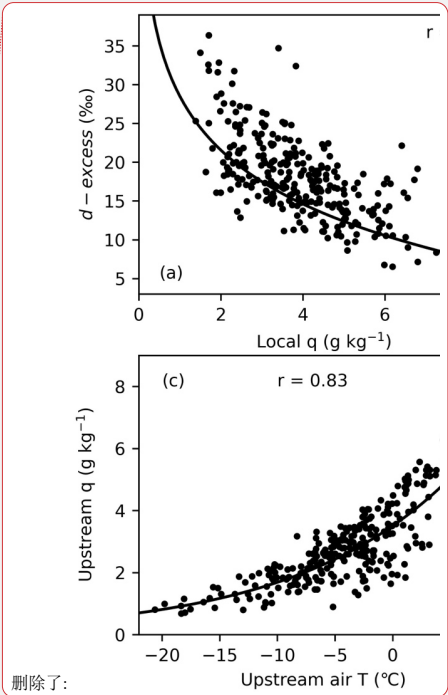


Figure 8. Relationships among vapor d -excess, local specific humidity (q), weighted-mean upstream q , weighted-mean upstream air temperature (T), and weighted-mean upstream air altitude during the non-monsoon season of November-April. (a) scatter plot of d -excess against local q . (b) scatter plot of local q against upstream weighted-mean q . (c) scatter plot of upstream q against upstream air T. (d) scatter plot of upstream q against upstream air altitude. All the upstream variables are mean values along backward trajectories weighted by the moisture contribution of air parcels. The solid curves indicate the log (a, c, and d) or linear (b) regression between the respective variables with the correlation coefficients indicated by the numbers.



删除了: d -excess

507 3.5 Role of rain-vapor interaction during the summer monsoon season

508 In contrast to the significant dependence of d -excess on q during the non-monsoon season, ~~no correlation is~~
509 ~~observed~~ ($r = 0.04$, $p = 0.51$) during the summer monsoon season. The behavior of $\delta^{18}\text{O}$ also differs between the
510 two seasons (Fig. 3). During the summer monsoon season, $\delta^{18}\text{O}$ - q plots below the Rayleigh curve, indicating that
511 the vapor has ~~experienced rain-vapor interaction through rain evaporation~~ (Fig. 3a). Partial rain evaporation in an
512 unsaturated atmospheric environment leads to kinetic fractionation, which decreases d -excess values in raindrops
513 while increasing d -excess in the surrounding vapor (Risi et al., 2008b). This effect of rain-vapor interaction on vapor
514 isotopes has been suggested as a primary mechanism driving the amount effect in tropical regions (Risi et al., 2008a;
515 Kurita et al., 2011; Bowen et al., 2019; Galewsky et al., 2016). Therefore, we hypothesize that vapor isotopes during
516 the summer monsoon season at SETP are influenced by the ~~extent~~ of rain-vapor interaction.

517 The first evidence supporting this hypothesis is the significant correlation between $\delta^{18}\text{O}$ and d -excess during
518 the summer monsoon season ($r = -0.55$, $p < 0.01$; Fig. 9a). In addition, $\delta^{18}\text{O}$ and d -excess ~~show a trend of weak~~
519 ~~correlation at high $\delta^{18}\text{O}$ values, but a stronger correlation when $\delta^{18}\text{O}$ values are low~~ (Figs. 9a and S9). To explore
520 this further, we categorized days with daily precipitation of at least 2 mm as “rainy days” and those with less than
521 2 mm as “non-rainy days”. This distinction is based on the premise that rain-vapor interaction cannot occur in the
522 absence of rainfall. The analysis reveals that $\delta^{18}\text{O}$ during rainy days is significantly lower than that during non-rainy
523 days, while d -excess show the opposite trend ($p < 0.01$ for both $\delta^{18}\text{O}$ and d -excess; Figs. 9b and 9c). Furthermore,
524 the correlation between $\delta^{18}\text{O}$ and d -excess becomes stronger on rainy days ($r = -0.69$, $p < 0.01$), though a weaker
525 negative correlation persists even on non-rainy days ($r = -0.40$, $p < 0.01$). Even when applying a stricter threshold
526 of 0 mm for non-rainy days, the negative correlation between $\delta^{18}\text{O}$ and d -excess remains significant ($r = -0.37$, $p <$
527 0.01). Moreover, correlations with local precipitation amount are weak for both $\delta^{18}\text{O}$ ($r = -0.31$, $p < 0.01$) and d -
528 excess ($r = 0.26$, $p < 0.01$). These findings lead us to infer that vapor isotopes during the summer monsoon season

删除了: vapor d -excess shows

删除了: with q

删除了: undergone a degree of rain-vapor interaction due to evaporation

删除了: degree

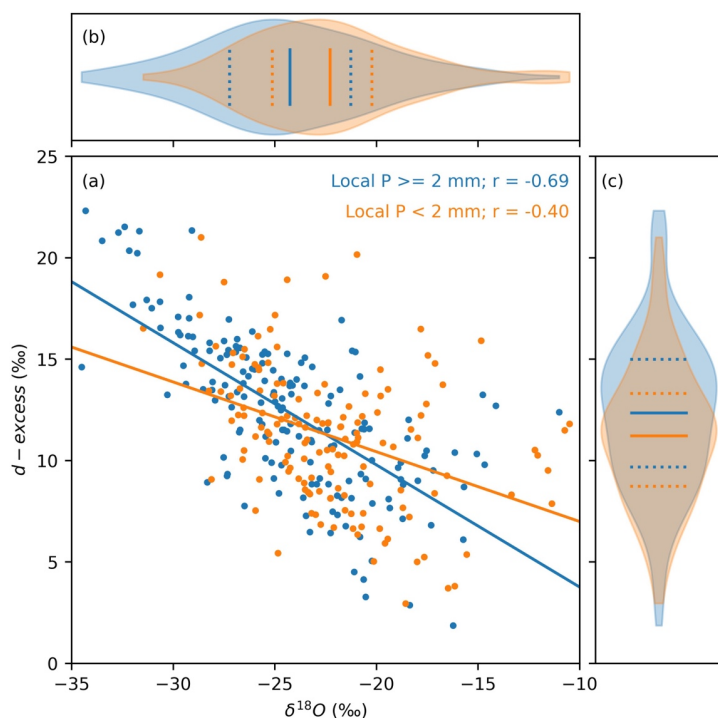
删除了:

删除了: there is a trend where

删除了: exhibit weaker correlations when $\delta^{18}\text{O}$ levels are high, and stronger correlations when $\delta^{18}\text{O}$ levels are low

删除了: S7

539 at SETP are influenced not only by local rain-vapor interactions but also by the history of rain-vapor interactions
 540 that occurred before the vapor reached the region.



541
 542 **Figure 9. Relationships between SETP vapor d -excess and $\delta^{18}\text{O}$ during the summer monsoon season. (a)**
 543 **scatter plot of d -excess against $\delta^{18}\text{O}$ and linear regression lines between them. (b) distribution of $\delta^{18}\text{O}$ values**
 544 **with the dashed lines indicate values at the lower and upper quartiles and the solid lines indicate the mean**
 545 **values. (c) is the same as (b) but for d -excess. Orange colors indicate data observed during daily precipitation**
 546 **amount less than 2 mm and blue colors indicate data observed during days with precipitation amount not**
 547 **less than 2 mm. The r values for both lines are indicated in (a) and both are significant at the 0.01 level.**

548 To further investigate the role of rain-vapor interactions, we use total precipitation amount (P_{acc}) as an indicator
 549 of rain-vapor interaction, considering the cumulative effect over several days preceding sampling. Our analysis

删除了: of them

551 examined correlations between vapor isotopes ($\delta^{18}\text{O}$ and d -excess) and P_{acc} over periods ranging from 1-10 days
552 prior to sampling (Figs. S10 and S11). Vapor d -excess reaches an optimal correlation with P_{acc} when considering 3
553 days before sampling (P_{acc_3d}). Vapor $\delta^{18}\text{O}$ shows a slightly longer memory and reaches an optimal correlation
554 around 5-6 days before sampling. Figure 10 shows the spatial distribution of these correlations, where d -excess
555 positively correlates with P_{acc_3d} across a $\sim 5^\circ \times 5^\circ$ region surrounding SETP and extending southwestward to the
556 Himalayas (Fig. 10a). In contrast, $\delta^{18}\text{O}$ shows significant negative correlations in similar regions (Fig. 10b).
557 Interestingly, even on non-rainy days, significant regional-scale correlations persist, albeit weaker and with a smaller
558 spatial extent (Fig. S12).
559 These findings provide further insights into understanding the mechanisms driving the amount effect. The
560 negative correlation between $\delta^{18}\text{O}$ and P_{acc} has also been observed in precipitation and can be attributed to either
561 continuous rainout (Ruan et al., 2019; Kurita et al., 2015; Cai and Tian, 2016) or rain-vapor interactions (Lawrence
562 et al., 2004; Risi et al., 2008a; Kurita et al., 2011; Worden et al., 2007). While continuous rainout, explained by the
563 Rayleigh distillation model, accounts for the decreasing trend of $\delta^{18}\text{O}$ with increased rainfall, d -excess remains
564 relatively stable unless specific humidity drops to very low levels ($\sim 4 \text{ g kg}^{-1}$ in Fig. 3b for example). The positive
565 correlation between vapor d -excess and P_{acc_3d} provides an additional constraint, suggesting that the amount effect
566 is not solely a result of rainout but also involves rain-vapor interactions, which significantly influence vapor isotopes
567 in the lower troposphere.

删除了: for

删除了: S8

删除了: S9

删除了: .

删除了: S10

删除了: evidence for

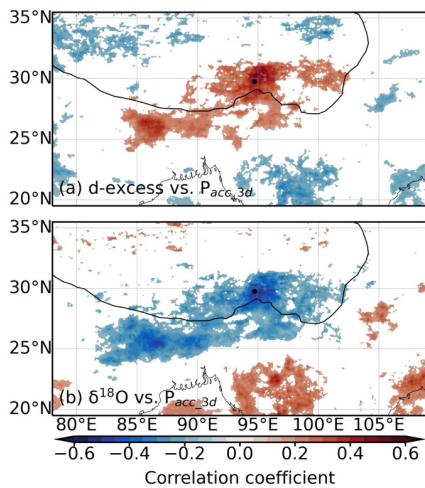


Figure 10. Relationships between vapor isotopes for rainy days (local daily precipitation amount not less than 2 mm) and total precipitation amount at the regional scale during the summer monsoon season. (a) spatial distribution of correlation coefficients between d -excess and total precipitation amount during 3 days prior sampling (P_{acc_3d}). (b) is the same as (a) but for $\delta^{18}O$. Only values significant at the 95% significance level are shown. The black dots indicate the location of the SETP station. The black solid lines denote the Tibetan Plateau with altitude contour at 3000 m.

4 Implications for interpreting TP ice core isotope data

Interpreting d -excess in meteoric water and ice cores on the TP is complicated by evaporation conditions over the northern Indian Ocean (RH_{SST} and SST) and continental recycling (Shao et al., 2021; Zhao et al., 2012; Joswiak et al., 2013; Pang et al., 2012; An et al., 2017). Attempts have been made to establish relationships between vapor d -excess and RH_{SST} (Chen et al., 2024; Liu et al., 2024), as well as between ice core d -excess and RH_{SST} (Shao et al., 2021) or SST (Zhao et al., 2012). Based on our results (Section 3.3), however, the apparent relationships are primarily a result of similarities in the seasonality of these variables. The preservation of oceanic source region

删除了: RH_{SST}

删除了: RH_{SST}

删除了: results in Section 3.3

591 conditions by vapor d -excess have also been questioned at other continental sites (Fiorella et al., 2018; Aemisegger
592 et al., 2014; Welp et al., 2012; Wei and Lee, 2019; Samuels - Crow et al., 2014). Instead, these studies emphasized
593 the role of other processes, such as continental recycling and mixing with subsiding air masses.

594 The direct contribution of oceanic vapor to humidity at SETP is very limited (Fig. 4), implying an even smaller
595 contribution over the TP since SETP is at the forefront of moisture transport toward TP (Fig. S1). The dominant
596 terrestrial origin indicates significant continental recycling. Terrestrial processes such as transpiration and
597 evaporation introduce isotopically enriched moisture with high d -excess signatures. Interestingly, vapor $\delta^{18}\text{O}$
598 exhibits a noticeable positive correlation with the fraction of within-boundary-layer moisture contribution over land
599 during the non-monsoon season ($r = 0.47$, $p < 0.01$), supporting that enhanced continental recycling would elevate
600 $\delta^{18}\text{O}$ values (Fig. 3a). However, correlations between the fraction of terrestrial moisture source and $\delta^{18}\text{O}$ for other
601 seasons or with d -excess are either insignificant or marginal (Table S1). Further quantification of the effect of
602 continental recycling on vapor isotopes requires detailed knowledge of the isotope compositions of
603 evapotranspiration fluxes. In this study, we utilized a simplified assumption regarding the isotopic composition of
604 these fluxes to explore their influence on vapor isotopes. Therefore, future research should prioritize characterizing
605 the isotopic signatures of both evaporation and transpiration fluxes, as well as determining the ratio between these
606 two fluxes. This will provide deeper insights into how continental recycling shapes vapor isotope compositions.

607 Seasonal changes and long-term variations in precipitation and ice core isotopes have been interpreted as shifts
608 in moisture source between recycled terrestrial moisture and oceanic sources or their relative contributions (An et
609 al., 2017; Yang and Yao, 2020). Oceanic moisture is typically associated with the summer monsoon, while westerlies
610 bring moisture from continental recycling or even the Mediterranean Sea. Water isotope signatures on the TP were
611 thought to reflect this interplay between the summer monsoon and non-monsoon seasons (Joswiak et al., 2013; Pang
612 et al., 2012; Tian et al., 2007). Despite seasonal shifts in moisture sources, continental recycling prevails throughout

删除了: Furthermore, t

删除了: and

删除了: , respectively

删除了: Mixing with terrestrial sources is also reflected in the relationship between vapor isotopes and q (Fig. 3).

删除了: westerlies

删除了: seasonally shifting

620 the year (Fig. 4). Our alternative perspective explains high d -excess induced by westerlies as dry and cold air
621 intrusions rather than surface evaporation or evapotranspiration. While the interplay between the summer monsoon
622 and westerlies remains valid, but we emphasize changes in air mass properties driven by different circulation
623 systems.

624 The proposed alternative interpretation aligns with findings from the Andes (Samuels - Crow et al., 2014) and
625 Corsica (Sodemann et al., 2017). potentially offering an explanation for the abnormally high d -excess in high-
626 altitude ice cores, as mentioned in the Introduction. This is because specific humidity at these ice core sites is
627 extremely low, and prolonged interaction with cold and dry air may further modify snow isotope compositions (Ma
628 et al., 2024; Wahl et al., 2022). In addition, intense rain-vapor interactions during the summer monsoon represent
629 another potential source of elevated d -excess (Section 3.5). When this high d -excess vapor contributes to subsequent
630 precipitation, its signal can be inherited in the resulting precipitation (Risi et al., 2008b). However, a clear
631 relationship between TP precipitation d -excess and monsoon convection has yet to be established, partly due to
632 limited attention paid to d -excess in previous studies (Yao et al., 2013). On the other hand, local raindrop evaporation
633 may counteract this effect by reducing raindrop d -excess values. The overall positive correlation between
634 precipitation d -excess and altitude across Asia has sometimes been attributed to stronger evaporation at lower
635 altitudes (Bershaw, 2018). For snowfall on glaciers, however, evaporation for falling snowflakes is less likely due
636 to cold temperatures and the short distance between the cloud base and the glacier surface. Therefore, elevated vapor
637 d -excess signals caused by accumulated rain-vapor interactions at upstream associated with monsoon convection
638 could be another possible source of the high d -excess in ice cores.

639 5 Conclusions

640 We present a three-year, daily near-surface vapor isotope dataset collected at the SETP station, which is at the

删除了: could also help explain

删除了: -long

删除了: observed

644 major channel for moisture entering the TP. The paired measurements of vapor isotopes and specific humidity reveal
645 distinct moisture sources and dynamics between non-monsoon and summer monsoon seasons, consistent with
646 findings from Lagrangian moisture diagnostic. Despite significant negative correlations between d -excess and
647 normalized RH over the northern Indian Ocean when all seasons are considered, these correlations weaken or even
648 disappear when analyzed within individual seasons. ▼

删除了: relative humidity

删除了: scaled to sea surface temperature

删除了: This finding challenges the earlier interpretation of TP d -excess as indicator of oceanic evaporation conditions and guarantees new interpretations in the future.

649 During the non-monsoon season, vapor d -excess is primarily influenced by specific humidity at both local and
650 upstream scales. Air that has undergone significant dehydration, situated at the lower end of the Rayleigh distillation,
651 is expected to have extremely high d -excess values. Backward trajectory analyses and moisture source diagnostics
652 reveal that the intrusion of cold and dry air driven by westerlies during the non-monsoon season leads to the
653 increasing trend in d -excess as specific humidity decreases. This process also contributes to a weak negative
654 correlation between d -excess and $\delta^{18}\text{O}$. Furthermore, $\delta^{18}\text{O}$ primarily reflects mixing processes involving a relatively
655 enriched moist end-member compared to the summer monsoon season. ▼

删除了: These new insights into vapor d -excess during the non-monsoon season provide an alternative framework for interpreting the high d -excess in high-altitude TP ice cores.

删除了: s

656 During the summer monsoon season, rain evaporation and “super-Rayleigh” processes emerge as the dominant
657 process shaping vapor isotope compositions. First, $\delta^{18}\text{O}$ systematically shifts below the Rayleigh distillation curve,
658 aligning with predictions of “super-Rayleigh” distillation caused by partial rain evaporation. Second, $\delta^{18}\text{O}$ is anti-
659 correlated with d -excess, pointing to kinetic fractionation as a source of depleted vapor, which cannot be attributed
660 solely to rainout. Third, at the regional scale, $\delta^{18}\text{O}$ shows significant negative correlations with total precipitation
661 amount, while d -excess positively correlates with total precipitation amount. ▼

删除了: These findings enhance our understanding of atmospheric humidity dynamics and help disentangle the different effects of rainout and rain-vapor interactions in the context of the amount effect.

662 These findings will aid in interpreting $\delta^{18}\text{O}$ and d -excess records from Tibetan Plateau glaciers, offering refined
663 insights into past hydroclimatic conditions and challenging assumptions linking ice core isotopes to oceanic
664 evaporation alone. The new insights into vapor d -excess during the non-monsoon season provide an alternative
665 framework for interpreting the high d -excess in high-altitude TP ice cores. The introduction of high d -excess values

删除了: This study reveals distinct moisture sources and dynamics between non-monsoon and monsoon seasons over the southeastern Tibetan Plateau.

682 by subsidence air from high altitudes could likely be a general phenomenon, as similar findings have been reported
683 elsewhere (Samuels - Crow et al., 2014; Sodemann et al., 2017). Additionally, the findings on summer monsoon
684 season moisture dynamics help disentangle the different effects of rainout and rain-vapor interactions in the context
685 of the amount effect (Bowen et al., 2019; Galewsky et al., 2016). While this study questions the earlier interpretation
686 of TP d -excess as an indicator of oceanic evaporation conditions (Zhao et al., 2012; Shao et al., 2021; Chen et al.,
687 2024; Liu et al., 2024), other studies have also raised doubts about the preservation of these signals inland (Fiorella
688 et al., 2018; Aemisegger et al., 2014; Welp et al., 2012; Wei and Lee, 2019; Samuels - Crow et al., 2014). Further
689 research is needed to determine how far inland oceanic evaporation signals can be preserved during the transport
690 from coastal areas. Moreover, we acknowledge the use of simplistic assumptions regarding the isotopic
691 compositions of evapotranspiration fluxes, highlighting the need for deeper investigation into the isotopic
692 compositions of these fluxes to comprehend the effect of continental recycling. Furthermore, the focus on lower
693 tropospheric vapor sources contrasts with precipitation sources at higher levels, which may differ and require
694 additional exploration. Finally, the resolution of meteorological data may influence the accuracy of trajectory
695 calculation and moisture tracking results. Future research should consider utilizing higher-resolution meteorological
696 data or implementing regional high-resolution models to enhance the precision of these analyses.

697 **Competing interests**

698 The authors declare that they have no conflict of interest.

699 **Acknowledgements**

700 We thank the editors and the referees for their comments and suggestions. This research was supported by the
701 National Key R&D Program of China (Grant 2024YFF0807901), the National Natural Science Foundation of China
702 (Grant 42371144), the Yunnan Fundamental Research Projects (Grant 202301AT070183), and the funding of

删除了: suggesetions

704 Donglu Talent Young Scholar from the Yunnan University and support for young scholars from the Double First-
705 Class Initiative for Ecological Disciplines of the Yunnan University. We would like to thank the staff at the South-
706 East Tibetan Plateau Station for integrated observation and research of alpine environment for their help in collecting
707 water samples and for sharing the meteorological data at the station.

708 **Data availability**

709 The NOAA ARL provided the HYSPLIT model and the GDAS data
710 (<https://www.ready.noaa.gov/HYSPLIT.php>). The Copernicus Climate Change Service provided the ERA5 data
711 (<https://doi.org/10.24381/cds.adbb2d47> and <https://doi.org/10.24381/cds.f17050d7>). The GPM data are available
712 through GES DISC (<https://doi.org/10.5067/GPM/IMERG/3B-HH/07>). Local meteorological data at the SETP
713 station are provided by National Tibetan Plateau / Third Pole Environment Data Center
714 (<https://dx.doi.org/10.11888/AtmosphericPhysics.tpe.68.db>). The observation data at the SETP station have been
715 uploaded to Figshare and will be made publicly available after publication (10.6084/m9.figshare.27302871).

716 **Author contributions**

717 **Zhongyin Cai**: Conceptualization, methodology, investigation, formal analysis, funding acquisition, writing-
718 original draft, writing-review & editing; **Rong Li**: Investigation, data curation, writing-review & editing; **Cheng**
719 **Wang**: Validation; **Qiukai Mao**: Investigation, **Lide Tian**: Resources, project administration, funding acquisition.

720 **References**

721
722 Aemisegger, F., Pfahl, S., Sodemann, H., Lehner, I., Seneviratne, S. I., and Wernli, H.: Deuterium excess as a
723 proxy for continental moisture recycling and plant transpiration, Atmos. Chem. Phys., 14, 4029-4054, 10.5194/acp-
724 14-4029-2014, 2014.
725 An, W., Hou, S., Zhang, Q., Zhang, W., Wu, S., Xu, H., Pang, H., Wang, Y., and Liu, Y.: Enhanced Recent Local

Moisture Recycling on the Northwestern Tibetan Plateau Deduced From Ice Core Deuterium Excess Records, *J. Geophys. Res.*, 122, 512,541–512,556, 10.1002/2017jd027235, 2017.

Araguás-Araguás, L., Fröhlich, K., and Rozanski, K.: Stable isotope composition of precipitation over southeast Asia, *J. Geophys. Res.*, 103, 28721–28742, 1998.

Benetti, M., Reverdin, G., Pierre, C., Merlivat, L., Risi, C., Steen-Larsen, H. C., and Vimeux, F.: Deuterium excess in marine water vapor: Dependency on relative humidity and surface wind speed during evaporation, *J. Geophys. Res.*, 119, 584–593, 2014.

Bershaw, J.: Controls on Deuterium Excess across Asia, *Geosciences*, 8, 257, 10.3390/geosciences8070257, 2018.

Bonne, J.-L., Behrens, M., Meyer, H., Kipfstuhl, S., Rabe, B., Schönike, L., Steen-Larsen, H. C., and Werner, M.: Resolving the controls of water vapour isotopes in the Atlantic sector, *Nature Communications*, 10, 1632, 10.1038/s41467-019-09242-6, 2019.

Bonne, J. L., Masson-Delmotte, V., Cattani, O., Delmotte, M., Risi, C., Sodemann, H., and Steen-Larsen, H. C.: The isotopic composition of water vapour and precipitation in Ivittuat, southern Greenland, *Atmos. Chem. Phys.*, 14, 4419–4439, 10.5194/acp-14-4419-2014, 2014.

Bony, S., Risi, C., and Vimeux, F.: Influence of convective processes on the isotopic composition ($\delta^{18}\text{O}$ and δD) of precipitation and water vapor in the tropics: 1. Radiative-convective equilibrium and Tropical Ocean–Global Atmosphere–Coupled Ocean–Atmosphere Response Experiment (TOGA-COARE) simulations, *J. Geophys. Res.*, 113, D19305, 10.1029/2008JD009942, 2008.

Bowen, G. J. and Wilkinson, B.: Spatial distribution of $\delta^{18}\text{O}$ in meteoric precipitation, *Geology*, 30, 315, 10.1130/0091-7613(2002)030<0315:sdoim>2.0.co;2, 2002.

Bowen, G. J., Cai, Z., Fiorella, R. P., and Putman, A.: Isotopes in the Water Cycle: Regional- to Global-Scale Patterns and Applications, *Annu. Rev. Earth Planet. Sci.*, 47, 453–479, 10.1146/annurev-earth-053018-060220, 2019.

Breitenbach, S. F. M., Adkins, J. F., Meyer, H., Marwan, N., Kumar, K. K., and Haug, G. H.: Strong influence of water vapor source dynamics on stable isotopes in precipitation observed in Southern Meghalaya, NE India, *Earth Planet. Sci. Lett.*, 292, 212–220, 10.1016/j.epsl.2010.01.038, 2010.

Cai, Z. and Tian, L.: Atmospheric controls on seasonal and interannual variations in the precipitation isotope in the East Asian Monsoon region, *J. Climate*, 29, 1339–1352, 10.1175/JCLI-D-15-0363.1, 2016.

Cai, Z. and Tian, L.: What causes the post-monsoon ^{18}O depletion over Bay of Bengal head and beyond?, *Geophys. Res. Lett.*, 47, e2020GL086985, 10.1029/2020gl086985, 2020.

Cai, Z., Tian, L., and Bowen, G. J.: ENSO variability reflected in precipitation oxygen isotopes across the Asian Summer Monsoon region, *Earth Planet. Sci. Lett.*, 475, 25–33, 10.1016/j.epsl.2017.06.035, 2017.

Cai, Z., Tian, L., and Bowen, G. J.: Spatial-seasonal patterns reveal large-scale atmospheric controls on Asian Monsoon precipitation water isotope ratios, *Earth Planet. Sci. Lett.*, 503, 158–169, 10.1016/j.epsl.2018.09.028, 2018.

Cai, Z., Li, R., Wang, C., and Tian, L.: Atmospheric controls on precipitation isotopes in North China and their response to record-breaking torrential rainfall, *J. Hydrol.*, 661, 10.1016/j.jhydrol.2025.133762, 2025.

Cao, R., Huang, H., Wu, G., Han, D., Jiang, Z., Di, K., and Hu, Z.: Spatiotemporal variations in the ratio of transpiration to evapotranspiration and its controlling factors across terrestrial biomes, *Agr. Forest Meteorol.*, 321, 108984, 10.1016/j.agrformet.2022.108984, 2022.

Chen, M., Gao, J., Luo, L., Zhao, A., Niu, X., Yu, W., Liu, Y., and Chen, G.: Temporal variations of stable isotopic compositions in atmospheric water vapor on the Southeastern Tibetan Plateau and their controlling factors, *Atmos. Res.*, 303, 10.1016/j.atmosres.2024.107328, 2024.

Craig, H.: Isotopic Variations in Meteoric Waters, *Science*, 133, 1702–1703, 10.1126/science.133.3465.1702,

1961.

Craig, H. and Gordon, L. I.: Deuterium and oxygen 18 variations in the ocean and the marine atmosphere, in: Stable Isotopes in Oceanographic Studies and Paleotemperatures. Spoleto, Tongiorgi, E., Italy, 9-130, 1965.

Dai, D., Gao, J., Steen-Larsen, H. C., Yao, T., Ma, Y., Zhu, M., and Li, S.: Continuous monitoring of the isotopic composition of surface water vapor at Lhasa, southern Tibetan Plateau, Atmos. Res., 264, 10.1016/j.atmosres.2021.105827, 2021.

Dansgaard, W.: Stable isotopes in precipitation, Tellus, 16, 436-468, 10.1111/j.2153-3490.1964.tb00181.x, 1964.

Dütsch, M., Pfahl, S., and Sodemann, H.: The impact of nonequilibrium and equilibrium fractionation on two different deuterium excess definitions, J. Geophys. Res., 122, 12732-12746, 10.1002/2017JD027085, 2017.

Fiorella, R. P., Poulsen, C. J., and Matheny, A. M.: Seasonal Patterns of Water Cycling in a Deep, Continental Mountain Valley Inferred from Stable Water Vapor Isotopes, J. Geophys. Res., 123, 7271-7291, doi:10.1029/2017JD028093, 2018.

Galewsky, J., Steen-Larsen, H. C., Field, R. D., Worden, J., Risi, C., and Schneider, M.: Stable isotopes in atmospheric water vapor and applications to the hydrologic cycle, Rev. Geophys., 54, 809-865, 10.1002/2015RG000512, 2016.

Good, S. P., Noone, D., and Bowen, G.: Hydrologic connectivity constrains partitioning of global terrestrial water fluxes, Science, 349, 175-177, 10.1126/science.aaa5931, 2015.

Guo, H., Pang, H., Wu, S., Xu, T., Mutz, S. G., Zhan, Z., Lin, W., Zhang, W., and Hou, S.: Global abnormal precipitation 18O depletion during late/post monsoon season, Earth Planet. Sci. Lett., 641, 10.1016/j.epsl.2024.118815, 2024.

Han, J., Tian, L., Cai, Z., Ren, W., Liu, W., Li, J., and Tai, J.: Season-specific evapotranspiration partitioning using dual water isotopes in a Pinus yunnanensis ecosystem, southwest China, J. Hydrol., 608, 127672, 10.1016/j.jhydrol.2022.127672, 2022.

He, S., Jackisch, D., Feng, L., Samanta, D., Wang, X., and Goodkin, N. F.: Uncovering Below Cloud Rain-Vapor Interactions During Tropical Rain Events Through Simultaneous and Continuous Real-Time Monitoring of Rain and Vapor Isotopes, J. Geophys. Res., 129, e2023JD040084, <https://doi.org/10.1029/2023JD040084>, 2024.

He, Y., Risi, C., Gao, J., Masson-Delmotte, V., Yao, T., Lai, C.-T., Ding, Y., Worden, J., Frankenberg, C., Chepfer, H., and Cesana, G.: Impact of atmospheric convection on south Tibet summer precipitation isotopologue composition using a combination of in situ measurements, satellite data and atmospheric general circulation modeling, J. Geophys. Res., 120, 3852-3871, 10.1002/2014JD022180, 2015.

Hersbach, H., Bell, B., Berrisford, P., Horányi, A., J., M.-S., Nicolas, J., Radu, R., Schepers, D., Simmons, A., Soci, C., and Dee, D.: Global reanalysis: goodbye ERA-Interim, hello ERA5, 10.21957/vf291hehd7, 2019.

Huang, J.: A Simple Accurate Formula for Calculating Saturation Vapor Pressure of Water and Ice, Journal of Applied Meteorology and Climatology, 57, 1265-1272, JAMC-D-17-0334.1, 2018.

Huffman, G. J., Stocker, E. F., Bolvin, D. T., Nelkin, E. J., and Tan, J.: GPM IMERG Final Precipitation L3 Half Hourly 0.1 degree x 0.1 degree V07, Greenbelt, MD, Goddard Earth Sciences Data and Information Services Center (GES DISC) [dataset], 10.5067/GPM/IMERG/3B-HH/07, 2023.

Immerzeel, W. W., Lutz, A. F., Andrade, M., Bahl, A., Biemans, H., Bolch, T., Hyde, S., Brumby, S., Davies, B. J., Elmore, A. C., Emmer, A., Feng, M., Fernández, A., Haritashya, U., Kargel, J. S., Koppes, M., Kraaijenbrink, P. D. A., Kulkarni, A. V., Mayewski, P. A., Nepal, S., Pacheco, P., Painter, T. H., Pellicciotti, F., Rajaram, H., Rupper, S., Sinisalo, A., Shrestha, A. B., Viviroli, D., Wada, Y., Xiao, C., Yao, T., and Baillie, J. E. M.: Importance and vulnerability of the world's water towers, Nature, 577, 364-369, 10.1038/s41586-019-1822-y, 2020.

Jiang, J., Zhou, T., Qian, Y., Li, C., Song, F., Li, H., Chen, X., Zhang, W., and Chen, Z.: Precipitation regime

changes in High Mountain Asia driven by cleaner air, *Nature*, 10.1038/s41586-023-06619-y, 2023.

Joswiak, D. R., Yao, T., Wu, G., Tian, L., and Xu, B.: Ice-core evidence of westerly and monsoon moisture contributions in the central Tibetan Plateau, *J. Glaciol.*, 59, 56-66, 10.3189/2013JoG12J035, 2013.

Keeling, C. D.: The concentration and isotopic abundances of atmospheric carbon dioxide in rural areas, *Geochim. Cosmochim. Acta*, 13, 322-334, 10.1016/0016-7037(58)90033-4, 1958.

Kurita, N., Fujiyoshi, Y., Nakayama, T., Matsumi, Y., and Kitagawa, H.: East Asian Monsoon controls on the inter-annual variability in precipitation isotope ratio in Japan, *Climate of the Past*, 11, 339-353, 10.5194/cp-11-339-2015, 2015.

Kurita, N., Noone, D., Risi, C., Schmidt, G. A., Yamada, H., and Yoneyama, K.: Intraseasonal isotopic variation associated with the Madden-Julian Oscillation, *J. Geophys. Res.*, 116, D24101, 10.1029/2010JD015209, 2011.

Lawrence, J. R., Gedzelman, S. D., Dexheimer, D., Cho, H.-K., Carrie, G. D., Gasparini, R., Anderson, C. R., Bowman, K. P., and Biggerstaff, M. I.: Stable isotopic composition of water vapor in the tropics, *J. Geophys. Res.*, 109, D06115, 10.1029/2003JD004046, 2004.

Lee, J.-E. and Fung, I.: "Amount effect" of water isotopes and quantitative analysis of post-condensation processes, *Hydrol. Processes*, 22, 1-8, 10.1002/hyp.6637, 2008.

Li, R., Cai, Z., Wang, C., Liu, F., Yang, D., Xu, C., Yu, S., Yu, X., Fan, Q., and Tian, L.: Multiple Climate Forcings Decomposed From a Tibetan Plateau Ice Core Isotope Record, *J. Geophys. Res.*, 130, e2024JD042929, <https://doi.org/10.1029/2024JD042929>, 2025.

Liu, F., Tian, L., Cai, Z., Wang, X., Liang, P., Wang, S., and Li, S.: What caused the lag between oxygen-18 and deuterium excess in atmospheric vapor and precipitation during the earlier summer season in southwest China?, *J. Hydrol.*, 644, 10.1016/j.jhydrol.2024.132087, 2024.

Liu, J., Xiao, C., Ding, M., and Ren, J.: Variations in stable hydrogen and oxygen isotopes in atmospheric water vapor in the marine boundary layer across a wide latitude range, *Journal of Environmental Sciences*, 26, 2266-2276, 10.1016/j.jes.2014.09.007, 2014.

Luo, L.: Meteorological observation data from the integrated observation and research station of the alpine environment in Southeast Tibet (2007-2017), National Tibetan Plateau Data Center [dataset], 10.11888/AtmosphericPhysics.tpe.68.db, 2018.

Ma, T., Jiang, Z., Ding, M., He, P., Li, Y., Zhang, W., and Geng, L.: A model framework for atmosphere-snow water vapor exchange and the associated isotope effects at Dome Argus, Antarctica – Part 1: The diurnal changes, *The Cryosphere*, 18, 4547-4565, 10.5194/tc-18-4547-2024, 2024.

Merlivat, L. and Jouzel, J.: Global climatic interpretation of the deuterium - oxygen 18 relationship for precipitation, *J. Geophys. Res.*, 84, 5029-5033, 1979.

Noone, D.: Pairing Measurements of the Water Vapor Isotope Ratio with Humidity to Deduce Atmospheric Moistening and Dehydration in the Tropical Midtroposphere, *J. Climate*, 25, 4476-4494, 10.1175/jcli-d-11-00582.1, 2012.

Pang, H., Hou, S., Kaspari, S., Mayewski, P., Introne, D., Masson-Delmotte, V., Jouzel, J., Li, Z., He, Y., Hong, S., and Qin, D.: Atmospheric circulation change in the central Himalayas indicated by a high-resolution ice core deuterium excess record, *Climate Research*, 53, 1-12, 10.3354/cr01090, 2012.

Putman, A. L., Fiorella, R. P., Bowen, G. J., and Cai, Z.: A Global Perspective on Local Meteoric Water Lines: Meta-analytic Insight into Fundamental Controls and Practical Constraints, *Water Resour. Res.*, 55, 6896-6910, 10.1029/2019wr025181, 2019.

Risi, C., Bony, S., and Vimeux, F.: Influence of convective processes on the isotopic composition ($\delta^{18}\text{O}$ and δD) of precipitation and water vapor in the tropics: 2. Physical interpretation of the amount effect, *J. Geophys. Res.*, 113, D19306, 10.1029/2008JD009943, 2008a.

858 Risi, C., Bony, S., Vimeux, F., Descroix, L., Ibrahim, B., Lebreton, E., Mamadou, I., and Sultan, B.: What controls
859 the isotopic composition of the African monsoon precipitation? Insights from event-based precipitation collected
860 during the 2006 AMMA field campaign, *Geophys. Res. Lett.*, 35, L24808, 10.1029/2008GL035920, 2008b.

861 Ruan, J., Zhang, H., Cai, Z., Yang, X., and Yin, J.: Regional controls on daily to interannual variations of
862 precipitation isotope ratios in Southeast China: Implications for paleomonsoon reconstruction, *Earth Planet. Sci.*
863 *Lett.*, 527, 115794, 10.1016/j.epsl.2019.115794, 2019.

864 Samuels-Crow, K. E., Galewsky, J., Sharp, Z. D., and Dennis, K. J.: Deuterium excess in subtropical free
865 troposphere water vapor: Continuous measurements from the Chajnantor Plateau, northern Chile, *Geophys. Res.*
866 *Lett.*, 41, 8652-8659, 10.1002/2014gl062302, 2014.

867 Shao, L., Tian, L., Cai, Z., Wang, C., and Li, Y.: Large-scale atmospheric circulation influences the ice core d-
868 excess record from the central Tibetan Plateau, *Clim. Dyn.*, 57, 1805-1816, 10.1007/s00382-021-05779-9, 2021.

869 Sodemann, H., Schwierz, C., and Wernli, H.: Interannual variability of Greenland winter precipitation sources:
870 Lagrangian moisture diagnostic and North Atlantic Oscillation influence, *J. Geophys. Res.*, 113,
871 10.1029/2007jd008503, 2008.

872 Sodemann, H., Aemisegger, F., Pfahl, S., Bitter, M., Corsmeier, U., Feuerle, T., Graf, P., Hankers, R., Hsiao, G.,
873 Schulz, H., Wieser, A., and Wernli, H.: The stable isotopic composition of water vapour above Corsica during the
874 HyMeX SOP1 campaign: insight into vertical mixing processes from lower-tropospheric survey flights, *Atmos.*
875 *Chem. Phys.*, 17, 6125-6151, 10.5194/acp-17-6125-2017, 2017.

876 Steen-Larsen, H. C., Risi, C., Werner, M., Yoshimura, K., and Masson-Delmotte, V.: Evaluating the skills of
877 isotope-enabled General Circulation Models against in-situ atmospheric water vapor isotope observations, *J.*
878 *Geophys. Res.*, 122, 246-263, 10.1002/2016JD025443, 2017.

879 Stein, A. F., Draxler, R. R., Rolph, G. D., Stunder, B. J. B., Cohen, M. D., and Ngan, F.: NOAA's HYSPLIT
880 atmospheric transport and dispersion modeling system, *Bull. Am. Meteorol. Soc.*, 96, 2059-2077, 10.1175/BAMS-
881 D-14-00110.1, 2015.

882 Terzer-Wassmuth, S., Wassenaar, L. I., Welker, J. M., and Araguas-Araguas, L. J.: Improved High-Resolution
883 Global and Regionalized Isoscapes of $\delta^{18}\text{O}$, $\delta^2\text{H}$, and d-Excess in Precipitation, *Hydrol. Processes*, 35,
884 10.1002/hyp.14254, 2021.

885 Thompson, L. G., Yao, T., E.Mosley-Thompson, Davis, M. E., Henderson, K. A., and Lin, P.-N.: A High-
886 Resolution Millennial Record of the South Asian Monsoon from Himalayan Ice Cores, *Science*, 289, 1916-1919,
887 10.1126/science.289.5486.1916, 2000.

888 Thompson, L. G., Yao, T. D., Davis, M. E., Mosley-Thompson, E., Sval, H. A., Wu, G., Bolzan, J. F., Kutuzov, S.,
889 Beaudon, E., Sierra-Hernández, M. R., and Beer, J.: Ice core evidence for an orbital-scale climate transition on the
890 Northwest Tibetan Plateau, *Quat. Sci. Rev.*, 324, 10.1016/j.quascirev.2023.108443, 2024.

891 Tian, L., Masson-Delmotte, V., Stievenard, M., Yao, T., and Jouzel, J.: Tibetan Plateau summer monsoon
892 northward extent revealed by measurements of water stable isotopes, *J. Geophys. Res.*, 106, 28081-28088,
893 10.1029/2001JD900186, 2001.

894 Tian, L., Yao, T., MacClune, K., White, J. W. C., Schilla, A., Vaughn, B., Vachon, R., and Ichianagi, K.: Stable
895 isotopic variations in west China: A consideration of moisture sources, *J. Geophys. Res.*, 112, D10112,
896 10.1029/2006jd007718, 2007.

897 Tian, L., Yu, W., Schuster, P. F., Wen, R., Cai, Z., Wang, D., Shao, L., Cui, J., and Guo, X.: Control of seasonal
898 water vapor isotope variations at Lhasa, southern Tibetan Plateau, *J. Hydrol.*, 580, 124237,
899 10.1016/j.jhydrol.2019.124237, 2020.

900 Uemura, R., Matsui, Y., Yoshimura, K., Motoyama, H., and Yoshida, N.: Evidence of deuterium excess in water
901 vapor as an indicator of ocean surface conditions, *J. Geophys. Res.*, 113, 10.1029/2008jd010209, 2008.

902 Wahl, S., Steen-Larsen, H. C., Hughes, A. G., Dietrich, L. J., Zühr, A., Behrens, M., Faber, A.-K., and Hörhold,
903 M.: Atmosphere-Snow Exchange Explains Surface Snow Isotope Variability, *Geophys. Res. Lett.*, 49,
904 e2022GL099529, 10.1029/2022GL099529, 2022.

905 Webster, C. R. and Heymsfield, A. J.: Water isotope ratios D/H, 18O/16O, 17O/16O in and out of clouds map
906 dehydration pathways, *Science*, 302, 1742-1745, 10.1126/science.1089496, 2003.

907 Wei, Z. and Lee, X.: The utility of near-surface water vapor deuterium excess as an indicator of atmospheric
908 moisture source, *J. Hydrol.*, 123923, 10.1016/j.jhydrol.2019.123923, 2019.

909 Welp, L. R., Lee, X., Griffis, T. J., Wen, X. F., Xiao, W., Li, S., Sun, X., Hu, Z., Val Martin, M., and Huang, J.: A meta-
910 analysis of water vapor deuterium-excess in the midlatitude atmospheric surface layer, *Global Biogeochem. Cycles*,
911 26, 10.1029/2011gb004246, 2012.

912 Worden, J., Noone, D., and Bowman, K.: Importance of rain evaporation and continental convection in the
913 tropical water cycle, *Nature*, 445, 528-532, 10.1038/nature05508, 2007.

914 Yang, X. and Yao, T.: Seasonality of moisture supplies to precipitation over the Third Pole: a stable water
915 isotopic perspective, *Sci Rep*, 10, 15020, 10.1038/s41598-020-71949-0, 2020.

916 Yang, X., Davis, M. E., Acharya, S., and Yao, T.: Asian monsoon variations revealed from stable isotopes in
917 precipitation, *Clim. Dyn.*, 51, 2267-2283, 10.1007/s00382-017-4011-4, 2017.

918 Yao, T., Masson-Delmotte, V., Gao, J., Yu, W., Yang, X., Risi, C., Sturm, C., Werner, M., Zhao, H., He, Y., Ren,
919 W., Tian, L., Shi, C., and Hou, S.: A review of climatic controls on $\delta^{18}\text{O}$ in precipitation over the Tibetan Plateau:
920 Observations and simulations, *Rev. Geophys.*, 51, 525-548, 10.1002/rog.20023, 2013.

921 Yao, T., Bolch, T., Chen, D., Gao, J., Immerzeel, W., Piao, S., Su, F., Thompson, L., Wada, Y., Wang, L., Wang, T.,
922 Wu, G., Xu, B., Yang, W., Zhang, G., and Zhao, P.: The imbalance of the Asian water tower, *Nature Reviews Earth
923 & Environment*, 3, 618-632, 10.1038/s43017-022-00299-4, 2022.

924 Yu, W., Tian, L., Ma, Y., Xu, B., and Qu, D.: Simultaneous monitoring of stable oxygen isotope composition in
925 water vapour and precipitation over the central Tibetan Plateau, *Atmos. Chem. Phys.*, 15, 10251-10262,
926 10.5194/acp-15-10251-2015, 2015.

927 Yu, W., Tian, L., Risi, C., Yao, T., Ma, Y., Zhao, H., Zhu, H., He, Y., Xu, B., Zhang, H., and Qu, D.: $\delta^{18}\text{O}$ records in
928 water vapor and an ice core from the eastern Pamir Plateau: Implications for paleoclimate reconstructions, *Earth
929 Planet. Sci. Lett.*, 456, 146-156, 10.1016/j.epsl.2016.10.001, 2016.

930 Zhang, Q., Shen, Z., Pokhrel, Y., Farinotti, D., Singh, V. P., Xu, C.-Y., Wu, W., and Wang, G.: Oceanic climate
931 changes threaten the sustainability of Asia's water tower, *Nature*, 615, 87-93, 10.1038/s41586-022-05643-8, 2023.

932 Zhang, Q., Shen, Z., Pokhrel, Y., Farinotti, D., Singh, V. P., Xu, C.-Y., Wu, W., and Wang, G.: Reply to: Atlantic
933 oceanic droughts do not threaten Asian water tower, *Nature*, 638, E16-E18, 10.1038/s41586-024-08358-0, 2025.

934 Zhao, H., Xu, B., Li, Z., Wang, M., Li, J., and Zhang, X.: Abundant climatic information in water stable isotope
935 record from a maritime glacier on southeastern Tibetan Plateau, *Clim. Dyn.*, 48, 1161-1171, 10.1007/s00382-016-
936 3133-4, 2017.

937 Zhao, H., Xu, B., Yao, T., Wu, G., Lin, S., Gao, J., and Wang, M.: Deuterium excess record in a southern Tibetan
938 ice core and its potential climatic implications, *Clim. Dyn.*, 38, 1791-1803, 10.1007/s00382-011-1161-7, 2012.

939 Zhao, Y., Xu, C., Yu, X., Liu, Y., and Ji, X.: Atlantic oceanic droughts do not threaten Asian water tower, *Nature*,
940 638, E13-E15, 10.1038/s41586-024-08357-1, 2025.

941

942